

Geology and physicochemical conditions of copper-gold mineralization at the Three Firs porphyry prospect, Woodjam district, south-central British Columbia

Shawn Vandekerkhove^{1, a}, Stephen M. Rowins^{1, 2, b}, and Stephen T. Johnston¹

¹School of Earth and Ocean Sciences, University of Victoria, Victoria, BC, V8P 5C2

²British Columbia Geological Survey, Ministry of Energy and Mines, Victoria, BC, V8W 9N3

^aDepartment of Earth Sciences, University of Toronto, ON, M5S 3B1

^bcorresponding author: Stephen.Rowins@gov.bc.ca

Recommended citation: Vandekerkhove, S., Rowins, S.M., and Johnston, S.T., 2014. Geology and physicochemical conditions of copper-gold mineralization at the Three Firs porphyry prospect, Woodjam district, south-central British Columbia. In: Geological Fieldwork 2013, British Columbia Ministry of Energy and Mines, British Columbia Geological Survey Paper 2014-1, pp. 67-94.

Abstract

The Three Firs prospect is one of six Cu-Au properties in the newly discovered Woodjam porphyry Cu-Au district of south-central British Columbia. It is hosted in Late Triassic volcanic and volcanoclastic rocks of the Nicola Group that form part of the southern Quesnel terrane, approximately 50 km northeast of Williams Lake. Copper-gold mineralization is spatially associated with medium-K, calc-alkaline, sub-vertical dikes ranging from monzonite to quartz monzonite in composition. Eight stages of vein formation and hydrothermal alteration are identified, with five stages directly associated with Cu-Au mineralization. Early potassic alteration occurs with stage 1 magnetite veins ("M" veins) and stage 2 hornblende ± actinolite veins. Main-stage veins include sinuous quartz-chalcopyrite-pyrite ± hornblende ± magnetite veins (stage 3 "A" veins) and straight, sharp-edged quartz-chalcopyrite-pyrite ± sercite ± hornblende ± magnetite veins with distinct medial suture lines (stage 4 "B" veins). Stages 3 and 4 veins are associated with calc-potassic and phyllic alteration, which replaces the earlier potassic alteration. Main-stage 5 sulphide stringer veins and veinlets consist of chalcopyrite-pyrite ± quartz, and are analogous to "D" veins in other calc-alkaline porphyry systems. Native gold has been found in the alteration halos of these veins. Stage 6 veins are weakly mineralized with open space crustification textures including layers of comb-textured quartz-carbonate ± sphalerite ± chalcopyrite ± pyrite ± tetrahedrite. These veins represent a minor carbonate-base metal stage of mineralization. Stage 7 veins consist of quartz ± pyrite ± carbonate ± epidote ± chlorite ± tourmaline and they are related to zones of propylitic alteration. The youngest veins recognized (stage 8) are unrelated to mineralization and consist of irregular and bifurcating calcite-ankerite veins. Fluid inclusion microthermometry indicates that the main stages of Cu-Au mineralization formed from saline (35 to 50 equiv. wt.% NaCl) aqueous fluids at temperatures between 300 and 400° C and pressures ranging from 0.6 to 1.42 kbar, which correspond to 2 to 4.6 km depth assuming lithostatic conditions. This P-T-X window is optimal for depositing Cu and Au, and exploration should continue to focus on the Three Firs area and its immediate environs. The Three Firs system is probably too deep for shallow, high-grade epithermal-style Au (Ag) zones, but there is the possibility, suggested by Au solubility studies, for slight enrichment of Au in zones immediately above the current level of Cu-Au mineralization.

Keywords: Porphyry, copper, gold, fluid inclusions, Jurassic, Triassic, Nicola arc, epithermal

1. Introduction

Copper in British Columbia is mined primarily from porphyry Cu-Au deposits, which accounted for \$1.5 billion in revenues, or 19% of the Province's mining sector, in 2012 (PriceWaterhouseCooper, 2012). Gold in these porphyry deposits is recovered as a byproduct of copper mining. In 2012 it accounted for \$275 million in revenues, or 4% of the mining sector. These porphyry Cu-Au deposits are hosted mainly in magmatic arc rocks of the Intermontane and Insular superterranes of the North American Cordillera (e.g., McMillan et al., 1996; Nelson et al., 2013). The focus of this paper is the newly discovered Three Firs porphyry prospect in the Woodjam porphyry Cu-Au district, approximately 50 km northeast of Williams Lake in south-central British Columbia (Fig. 1).

Three Firs was discovered by exploration drilling of a subsurface magnetic anomaly by Gold Fields Canada in the summer of 2012. The Woodjam district is in the Quesnel terrane, which forms part of the large Intermontane superterrane

that hosts numerous porphyry Cu-Mo-Au deposits, including Highland Valley Copper, Copper Mountain, Mount Polley, and Gibraltar (Fig. 2). The district hosts several other porphyry prospects including Deerhorn, Spellbound, Takom, Megabuck, and the Southeast Zone (Blackwell et al., 2012a; Sherlock et al., 2013). It is unusual because it potentially hosts both calc-alkaline and alkalic styles of porphyry Cu-Au mineralization (e.g., Blackwell et al., 2012a; del Real et al., 2013; Sherlock et al., 2013). The potential alkalic porphyry Cu-Au deposits include Deerhorn and Megabuck, whereas the Southeast Zone, Spellbound, Takom and Three Firs are considered calc-alkaline systems (del Real et al., 2013; Sherlock et al., 2013).

Herein we document the mineralogy and morphology of the veins and attendant alteration that constitute the main stages of Cu-Au mineralization at the Three Firs prospect, based on graphical logs from diamond drill core, petrographic examination, whole-rock geochemical analyses, and reflectance spectroscopy. To quantify the physicochemical

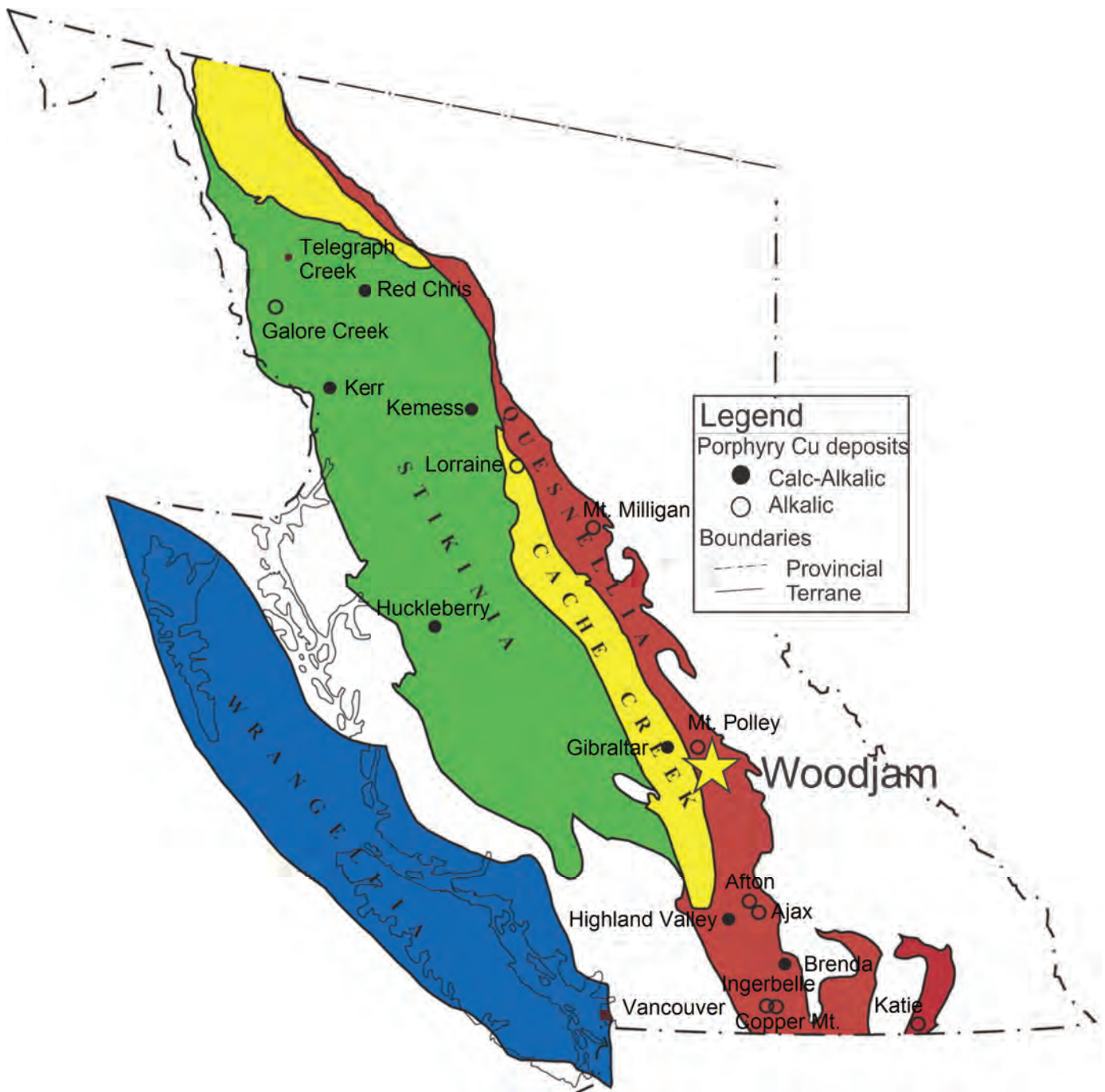


Fig. 1. Distribution of calc-alkaline and alkalic porphyry Cu±Mo±Au deposits and terranes with porphyry deposits in British Columbia.

conditions of the main Cu-Au mineralization event(s), we also present a microthermometric analysis of fluid inclusions in hydrothermal quartz from mineralized veins. Derived pressure, temperature, and fluid composition data can be useful vectors to undiscovered zones of mineralization. These data also permit a better evaluation of the ultimate ore potential (size and tonnage) of the magmatic-hydrothermal system.

We conclude that the Three Firs prospect is a Late Triassic-Early Jurassic calc-alkaline porphyry Cu-Au deposit that formed from saline (35 to 50 equivalent wt.% NaCl), aqueous

brines depositing metals in quartz-chalcopyrite-bornite-pyrite veins at 300 to 400° C, and 0.6 to 1.42 kb (2 to 4.6 km depth, assuming lithostatic load). These physicochemical conditions are within the favourable pressure-temperature-compositional window for the formation of porphyry Cu-Au deposits (e.g., Hezarkhani et al., 1999).

2. Geological setting

The Canadian Cordillera consists of five major morphological belts that are aligned north to northwest, approximately parallel

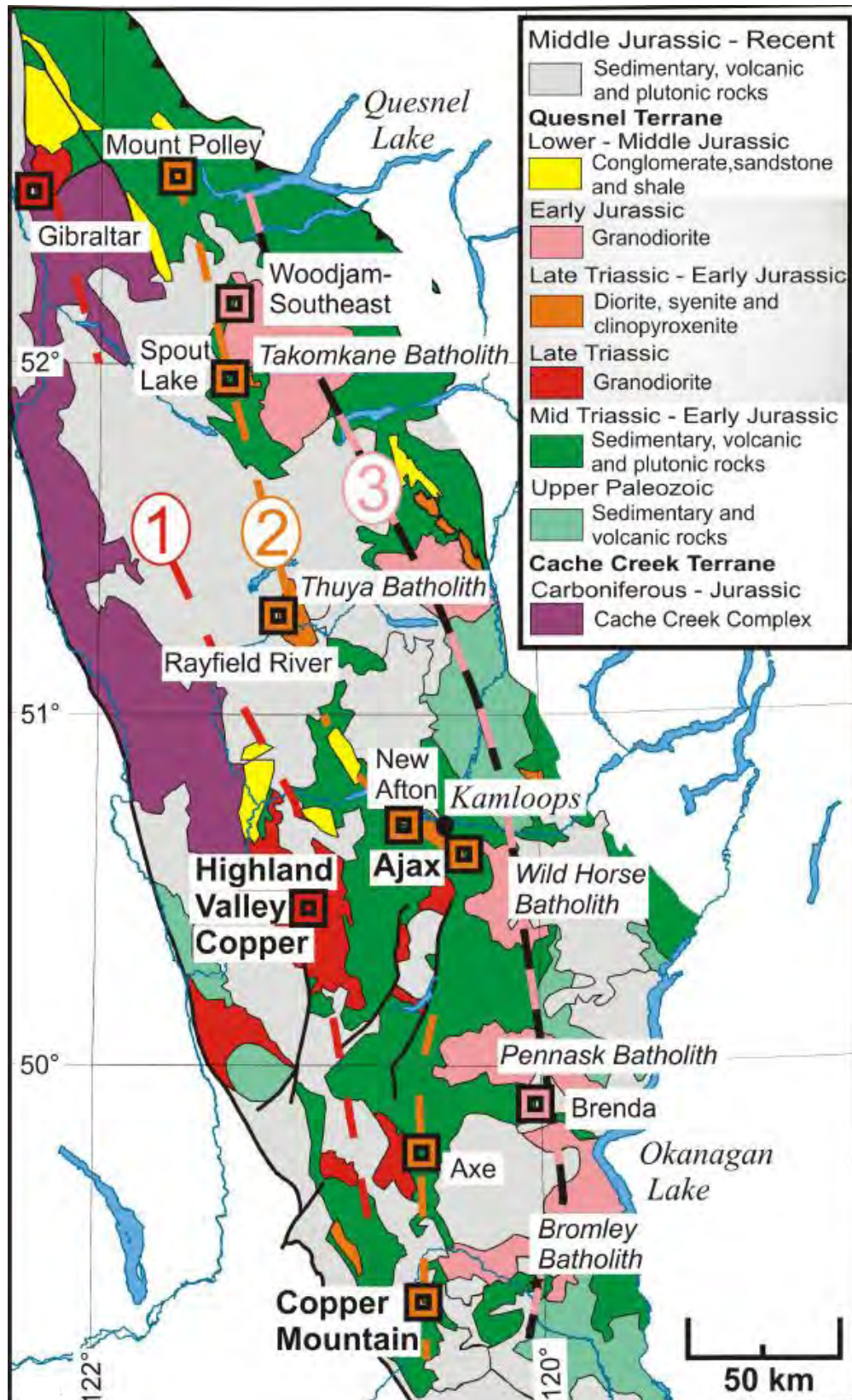


Fig. 2. Generalized geology of southern Quesnellia and porphyry Cu (Mo, Au) deposits. Mesozoic arc plutons align along the length of southern Quesnellia and define three north-trending, temporally distinct belts that young to the east: (1) Late Triassic; (2) Late Triassic – Early Jurassic; and (3) Early Jurassic. Discrete porphyry Cu (Mo, Au) mineralization events are linked directly to each of these magmatic episodes (after Logan, 2013).

to the margin of ancestral North America and the present-day coastline (Gabrielse and Yorath, 1991). From west to east they are the Insular, Coast, Intermontane, Omenica, and Foreland belts (Fig. 1). Porphyry-style mineralization in the Canadian Cordillera has a strong spatial correlation with the Intermontane and Insular superterrane, with the latter hosting most porphyry deposits (e.g., McMillan et al., 1995). Quesnel terrane, in the south-central part of the Intermontane superterrane, consists of upper Paleozoic and lower Mesozoic rocks. The Paleozoic components display oceanic and volcanic arc affinity and are unconformably overlain by Late Triassic and Early Jurassic island arc rocks of the Nicola and Takla groups (McMillan et al., 1995). Overlying the Early Jurassic volcanic arc rocks are lower to middle Jurassic siliciclastic rocks (Schiarrizza et al., 2009).

Preto (1977) recognized two parallel, north-trending, magmatic belts in the southern part of Quesnellia. Plutonism in the western belt is calc-alkaline and related to porphyry Cu-Mo mineralization, whereas in the eastern belt it is alkaline and related to porphyry Cu-Au mineralization. Logan et al. (2011) expanded this model and proposed that the eastward migration of Mesozoic arc magmatism led to the growth of three temporally distinct, north-trending, plutonic belts. From west to east these are (Fig. 2): the Guichon Creek suite (212–208 Ma, Late Triassic); the Copper Mountain suite (206–200 Ma, Late Triassic–Early Jurassic); and the Takomkane suite (197–193 Ma, Early Jurassic). All three magmatic belts contain porphyry-style mineralization, with the middle Copper Mountain suite associated with alkalic porphyry Cu-Au deposits. The Woodjam porphyry, a sub-unit of the Takomkane batholith is 197 Ma, as reported in Logan et al. (2011). However, application of this model in the Woodjam district is potentially problematic if both calc-alkaline and alkalic styles of porphyry Cu-Au mineralization exist (e.g., Blackwell et al., 2012a; del Real et al., 2013; Sherlock et al., 2013) because it implies that the Late Triassic–Early Jurassic (Copper Mountain suite) and the Early Jurassic (Takomkane suite) magmatic belts overlapped in this part of the southern Nicola arc. This is inconsistent with an easterly migrating magmatic arc. Alternatively, additional work may reveal that the proposed alkalic prospects in the Woodjam camp (Deerhorn and Megabuck) are actually calc-alkaline porphyry Cu-Au systems that belong to the Early Jurassic Takomkane suite.

Regional 1: 100,000 scale geological mapping of the Three Firs area was carried out by Bailey et al. (1990) and more detailed maps were made by Panteleyev et al. (1996), Logan et al. (2007), and Blackwell et al. (2012a). The Three Firs prospect is hosted in volcanoclastic rocks of the Nicola Group (Triassic–Jurassic; Fig. 3). The Nicola Group is intruded by the Takomkane batholith (Late Triassic–Early Jurassic), which is exposed in the southeast part of the property. Volcanic units of the Nicola Group are pervasively hornfelsed adjacent to the Takomkane batholith, and commonly contain abundant metamorphic epidote and tourmaline. Late Miocene olivine-phyric basaltic flows of the Chilcotin Group overlie the Nicola Group immediately west of the Three Firs prospect (Fig. 3). Late Wisconsin glaciolacustrine and glaciofluvial sediments cover all but a small portion of the Woodjam property.

3. Recent exploration history

Copper-gold mineralization at Three Firs consists of fine-grained sulphide disseminations and quartz-sulphide veins containing mainly chalcopyrite and, locally, bornite. Native Au was observed in disseminated grains of chalcopyrite. Mineralized quartz vein stockworks are hosted primarily in volcanic and volcanoclastic units, monzonite dikes, and quartz monzonite dikes that intrude the host stratigraphy. Early (pre-mineralization) and late (syn- to post-mineralization) dikes are also recognized on the property.

A complete exploration history of the Woodjam district is given in Sherlock et al. (2013). Briefly, the Three Firs prospect is part of the Woodjam North claim, a property 49% owned by Consolidated Woodjam Copper Corporation (formerly the Woodjam Joint Venture, which is a 60:40 ownership agreement between Fjordland Exploration Inc. and Cariboo Rose Resources Ltd.) and 51% owned by Gold Fields Horsefly Exploration Corporation (Gold Fields) a member of the Gold Fields group of companies. The Woodjam district has been explored numerous times since the late 1800s by multiple companies with varying exploration objectives. The area became a true exploration play, however, with the discovery of the Southeast Zone in 2007 (Fig. 4). A ground geophysical program of IP chargeability, resistivity, and ground magnetics highlighted an anomalous IP chargeability response in a new area, now known as the Southeast Zone (Fig. 4). A drill hole to test this IP anomaly (07-79) graded 0.34% Cu, 0.05 g/t Au, and 0.014% Mo over 203.55 m, with the upper 113.8 m returning 0.40% Cu, 0.05 g/t Au and 0.014% Mo. Further drilling and geophysical surveys led to the discovery of the Deerhorn zone in 2008. In 2011 Gold Fields acquired the Three Firs area (previously called the Megalloy area) and did a soil geochemical survey in conjunction with an expanded IP chargeability and ground magnetic survey. Drilling a coincident IP chargeability and magnetic high in 2012 resulted in discovery of the Three Firs prospect. The third drill hole (MAG12-03) of the program returned 177 m grading 0.21% Cu and 0.14 g/t Au or 0.59 g/t Au equivalent (Fig. 5).

4. Geology of the Three Firs prospect

4.1. Methods

In August 2012, four diamond-drill holes, MAG12-02, MAG12-03, MAG12-04 and MAG12-05 were logged at one-metre intervals. Core logging focused on determining: 1) alteration styles; 2) vein types, orientations, and mineral assemblages; and 3) lithological units and contacts. Core logs and accompanying 43-element assay results including Au, Cu, and As, collected previously at regular sample intervals along the length of the core, were then matched. The resultant graphical core logs were used to construct a factual geological cross-section across the Three Firs prospect. We collected 37 HQ diamond drill core samples representing the types of mineralization, veins, and rock types from all four of the MAG series drill holes. We paid particular attention to samples exhibiting crosscutting relationships that could constrain hydrothermal fluid events related to metal deposition and vein paragenesis. Thin section off-cuts were stained with sodium cobalt nitrate acid to distinguish between potassium feldspar, plagioclase, and quartz. Polished thin sections were examined to identify minerals, point count modal abundances, establish

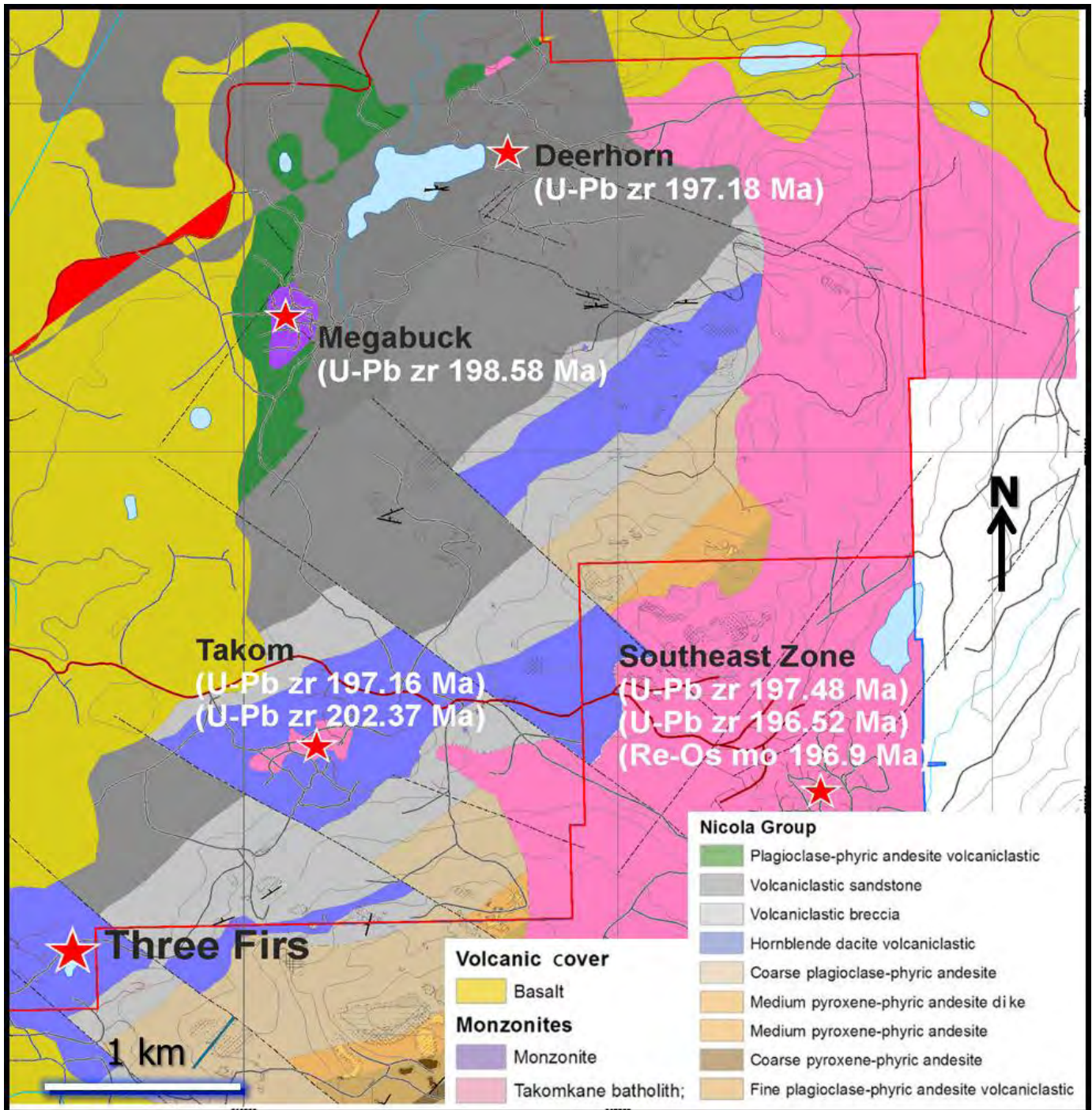


Fig. 3. Local geology of the Three Firs prospect (after Blackwell et al., 2012a; del Real et al., 2013). Geochronology from Schiarizza et al. (2009), Logan et al. (2011) and Blackwell et al. (2012a, and references therein).

textures, and document mineral paragenesis.

4.2. Overview

Volcanic and volcanoclastic rocks of the Nicola Group (~204 Ma; Figs. 6, 7) are oriented approximately $214^\circ / 30^\circ$ (Logan et al., 2011). The base of the Nicola section is defined by coarse-grained plagioclase-phyric andesite. At the top of this unit, a hyaloclastic bed in contact with volcanic sandstones displays pepperite structures indicating that the section is right way up,

as suggested by regional mapping (Bailey et al., 1990). The Nicola Group is cut by the ~197 Ma Takomkane batholith (Schiarizza et al., 2009; Logan et al., 2011) that outcrops to the east (Fig. 3). Several quartz-biotite monzonite, quartz monzonite, and monzonite dikes intrude the Nicola Group and are spatially associated with the best zones of mineralization. The orientation of the dikes suggests emplacement approximately perpendicular to stratigraphy, similar to that at the Megabuck Cu-Au porphyry prospect (Sherlock et al., 2013).

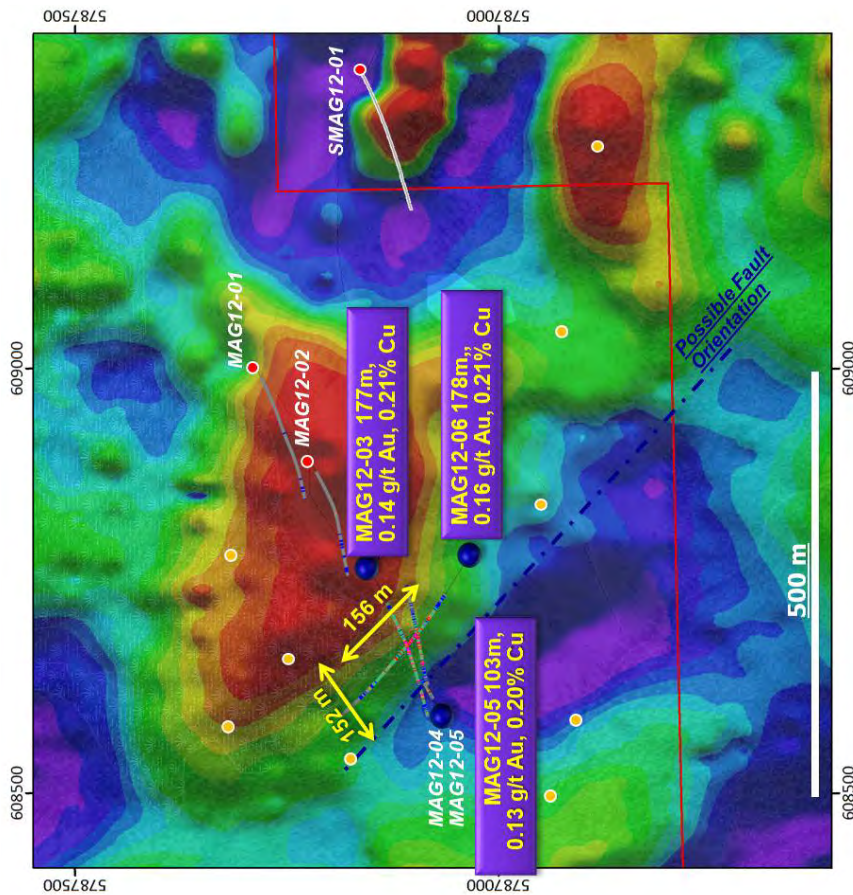


Fig. 5. Ground magnetic image of the Three Firs property, Blackwell et al. (2012a). UTM Zone 10, NAD83.

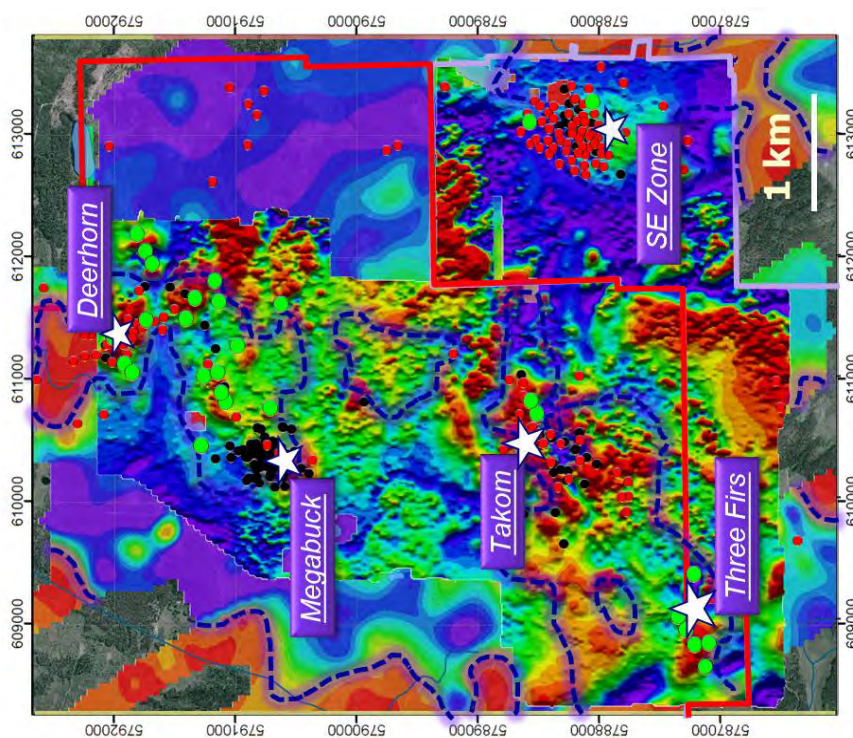


Fig. 4. Ground magnetic image of the Woodjam North property, modified from Sherlock (2013). UTM Zone 10, NAD83.

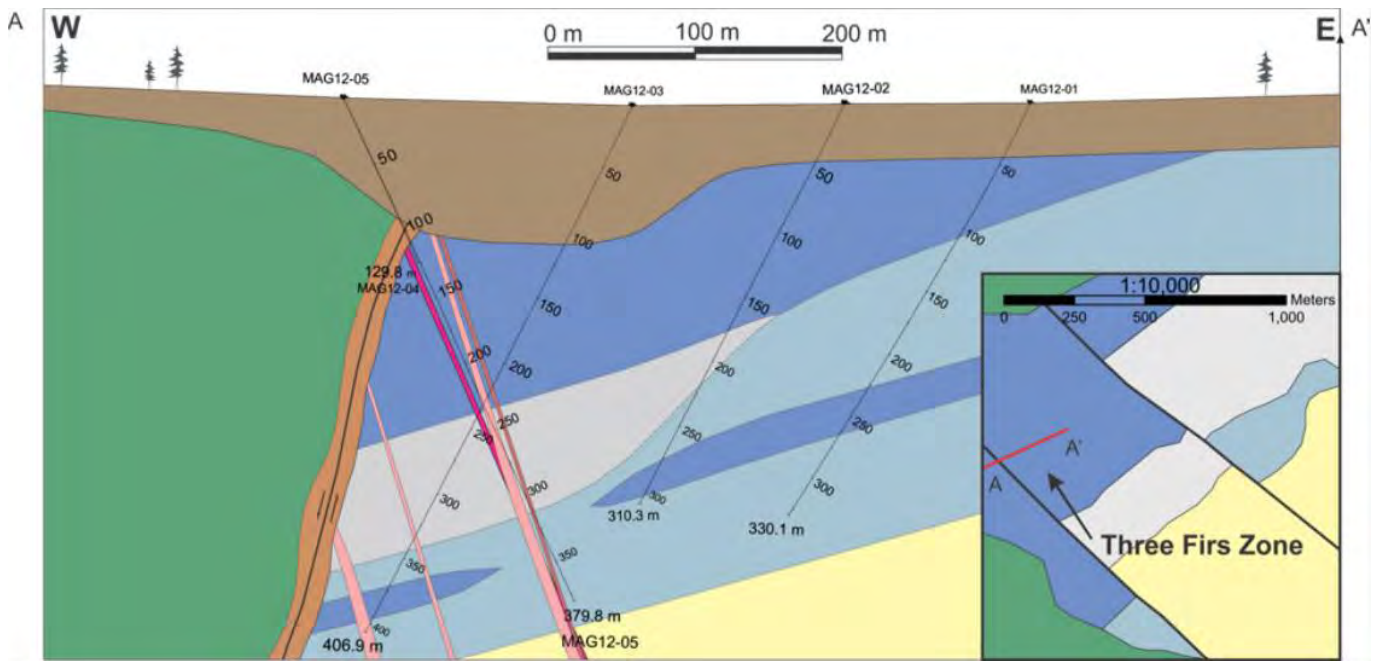


Fig. 6a. Cross-section of the Three Firs prospect (after Vandekerkhove, 2013).



Fig. 6b. Legend of the Three Firs lithologies in cross-section.

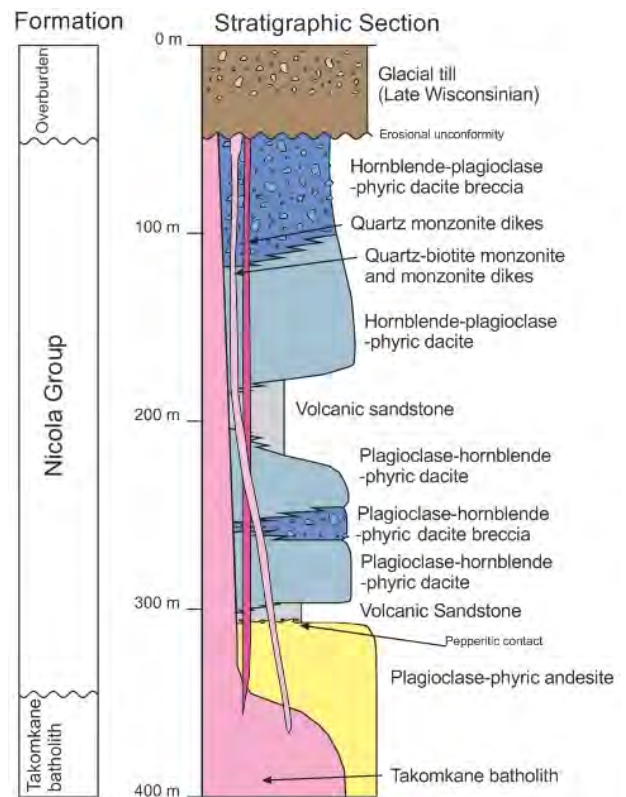


Fig. 7. Stratigraphic section of the Three Firs area.

4.3. Nicola Group host rocks

At Three Firs, the Nicola Group consists of four interfingering facies: plagioclase-phyric andesite; plagioclase-hornblende-phyric dacite; plagioclase-hornblende-phyric dacite breccia; and massive volcanic sandstone (Figs. 6, 7).

4.3.1. Plagioclase-phyric andesite

Plagioclase-phyric andesite is a visually distinctive unit with euhedral laths of greyish white plagioclase up to 2 cm long enclosed in a massive, fine-grained groundmass of dark grey plagioclase, quartz, and amphibole that is variably altered to sericite, chlorite and minor calcite. The upper contact of the unit displays pepperitic textures. A locally well developed trachytic texture defined by the alignment of plagioclase phenocrysts gives this unit the colloquial name of “Turkey Track” andesite (Blackwell et al., 2012a).

4.3.2. Plagioclase-hornblende-phyric dacite

Plagioclase-hornblende-phyric dacite has a speckled appearance and is medium to very dark grey, massive, and strongly magnetic (Fig. 8). Elongate, subhedral to euhedral,

plagioclase phenocrysts (< 5 mm long), and prismatic, subhedral to euhedral, hornblende phenocrysts (< 5 mm long) are enclosed in a groundmass of fine-grained quartz, amphibole, and plagioclase. This unit exhibits gradational contacts with both plagioclase-hornblende-phyric dacite breccia and massive volcanic sandstone. Felsic dikes with sharp contacts locally intrude the dacite.

4.3.3. Plagioclase-hornblende-phyric dacite breccia

Plagioclase-hornblende phyric dacite breccia is typically strongly magnetic, medium to very dark grey, with sub-angular to angular monolithic clasts 2 to 10 cm in diameter supported in a sand-sized matrix that is rich in plagioclase crystals (Fig. 9). Clasts and matrix exhibit similar mineralogy to the plagioclase-hornblende-phyric dacite unit. Crystal fragments of plagioclase in the matrix, together with the angularity of the clasts, imply that this unit is an autoclastic breccia derived from the plagioclase-hornblende-phyric dacite. The breccia displays gradational contacts with plagioclase-hornblende-phyric dacite and massive volcanic sandstone, and is locally intruded by felsic dikes with sharp contacts.

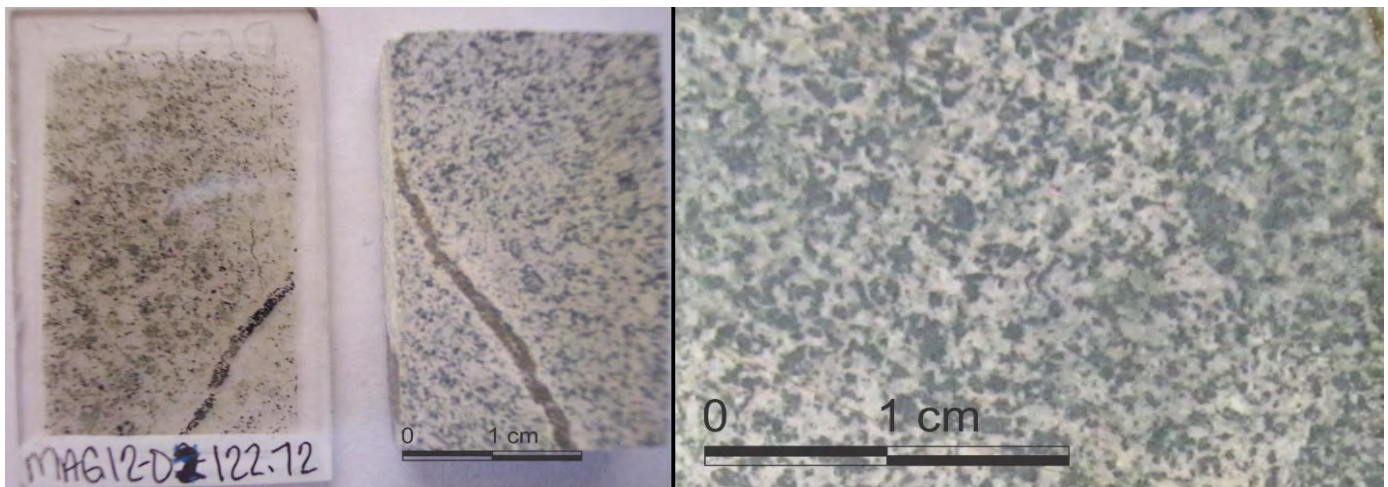


Fig. 8. Plagioclase-hornblende-phyric dacite. Thin section (left), stained off-cut (centre) and hand sample (right) taken from MAG12-02 at 122.72 m depth.

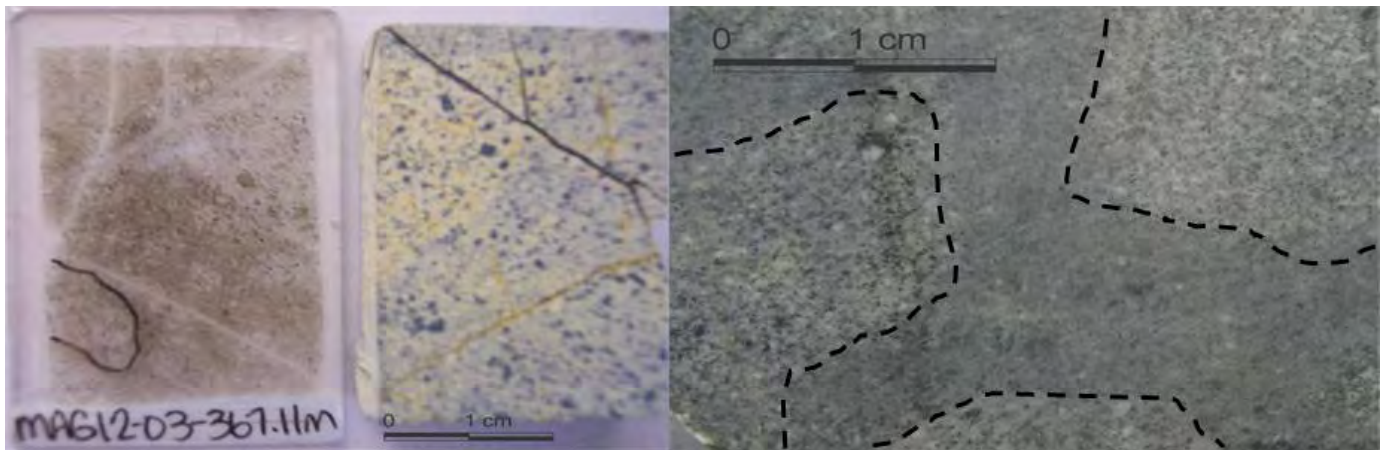


Fig. 9. Plagioclase-hornblende-phyric dacite breccia. Thin section (left) and stained off-cut (centre) taken from MAG12-03 at 367.11 m. Hand sample (right) taken from MAG12-02 at 231.50 m. Breccia fragments in hand sample outlined by dashed lines.

4.3.4. Massive volcanic sandstone

This unit is dark grey, massive, and commonly strongly magnetic. The texturally and compositionally immature plagioclase crystal-rich framework (< 5 mm) is very similar in appearance (Fig. 10) to the clast-supporting matrix in the dacite breccia (Fig. 9). Volcanic sandstones display gradational contacts with other volcanic and volcanoclastic units, and are similarly intruded by felsic dikes possessing sharp intrusive contacts.

4.4. Intrusive dikes

4.4.1. Quartz monzonite

Medium-grained quartz monzonite dikes intrude all volcanic and volcanoclastic Nicola Group units at Three Firs. Dikes

display sharp, but irregular contacts that crosscut mineralized main-stage veins (below) indicating post-mineralization emplacement. Quartz monzonite dikes are weakly porphyritic, light pink, and variably mottled (Fig. 11). They contain euhedral to subhedral plagioclase phenocrysts 3 to 5 mm in diameter, subhedral K-feldspar phenocrysts < 3 mm in diameter, rare quartz crystals < 2 mm in diameter, and subhedral hornblende (nearly completely replaced by chlorite) in a fine-grained groundmass of quartz, plagioclase, and K-feldspar.

4.4.2. Quartz-biotite monzonite

Quartz-biotite monzonite dikes locally intrude the Nicola Group, displaying sharp irregular contacts. These contacts are cut by mineralized veins, indicating that emplacement was

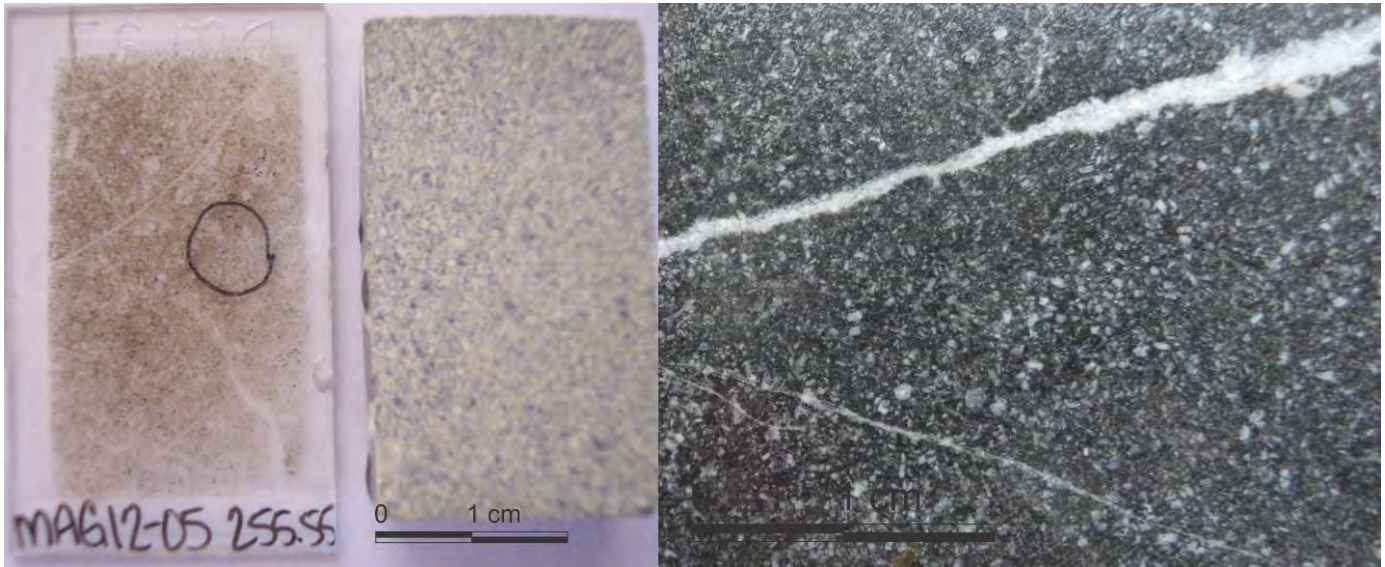


Fig. 10. Massive volcanic sandstone. Thin section (left), stained off-cut (centre) and hand sample (right) are all taken from MAG12-05 at 255.55 m depth.

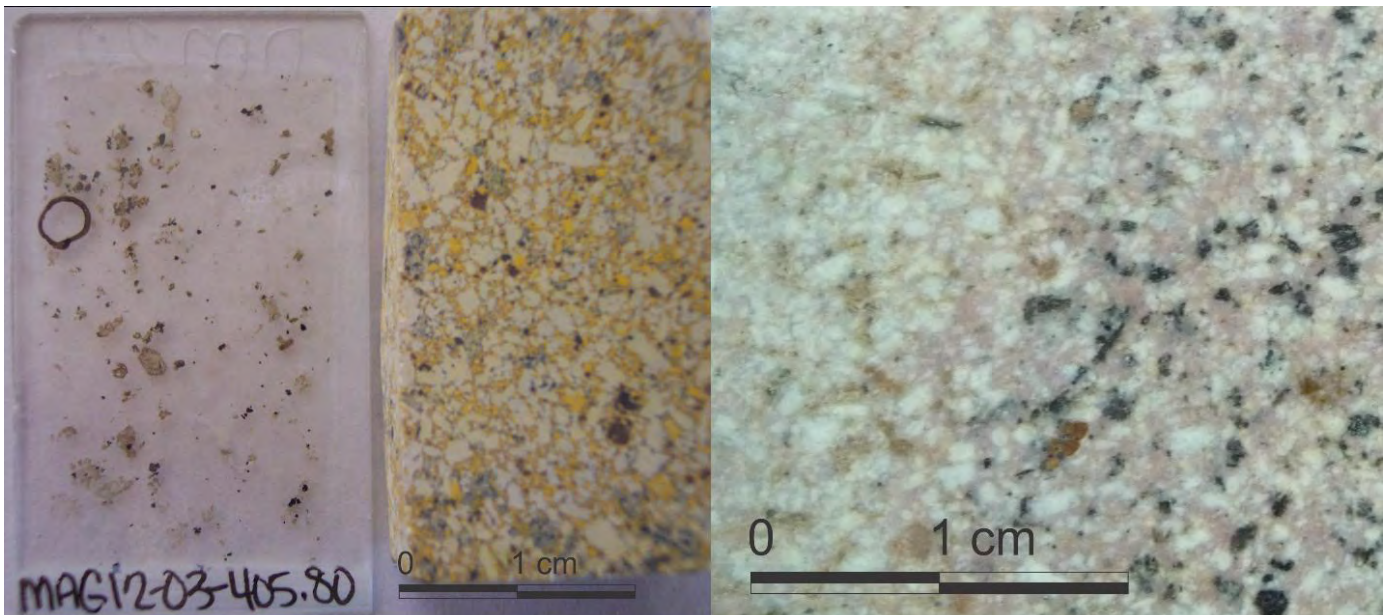


Fig. 11. Quartz monzonite dike. Thin section (left), stained off-cut (centre) and hand sample (right) are all taken from MAG12-03 at 405.80 m depth. Note the sericite and chlorite alteration of the left side of the hand sample.

pre-mineralization. The dikes are medium grained, and light greyish pink to dark grey (Fig. 12). They are weakly porphyritic and contain euhedral to subhedral plagioclase phenocrysts (3-5 mm in diameter), anhedral biotite (1-3 mm in diameter), and rare subhedral K-feldspar (1-2 mm in diameter). The fine-grained groundmass consists of plagioclase, quartz, K-feldspar, and minor biotite. Where altered, biotite phenocrysts and groundmass are replaced mainly by chlorite and clay minerals.

4.4.3. Monzonite

Monzonite dikes are medium grained and consist of weakly porphyritic hornblende, biotite, plagioclase, and

lesser K-feldspar in a fine-grained groundmass of K-feldspar, plagioclase, and minor quartz. Biotite is subhedral, shreddy and largely replaced by chlorite. Elongate prismatic crystals of hornblende are similarly replaced by chlorite. Plagioclase forms both elongate euhedral laths and stubby subhedral tablets. Less abundant K-feldspar phenocrysts are equant with euhedral to subhedral habits. All phenocrysts are 2 to 5 mm long. Intrusive contacts (Fig. 13) display chilled margins with an increased abundance of fine-grained quartz and K-feldspar. Monzonite dikes both cut and are crosscut by mineralized quartz veins (Fig. 13), indicating that the monzonite was emplaced coeval with mineralization.

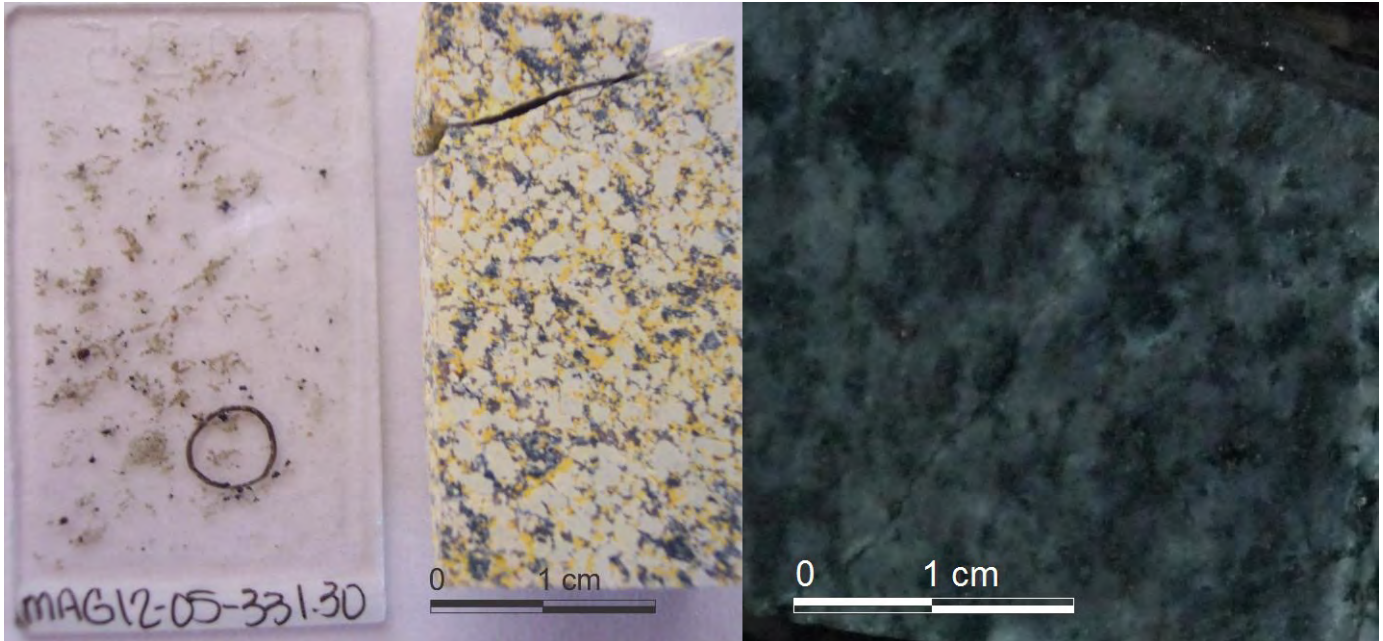


Fig. 12. Quartz-biotite monzonite dike. Thin section (left), stained off-cut (centre), and hand sample (right) are all taken from MAG12-05 at 331.30 m depth.

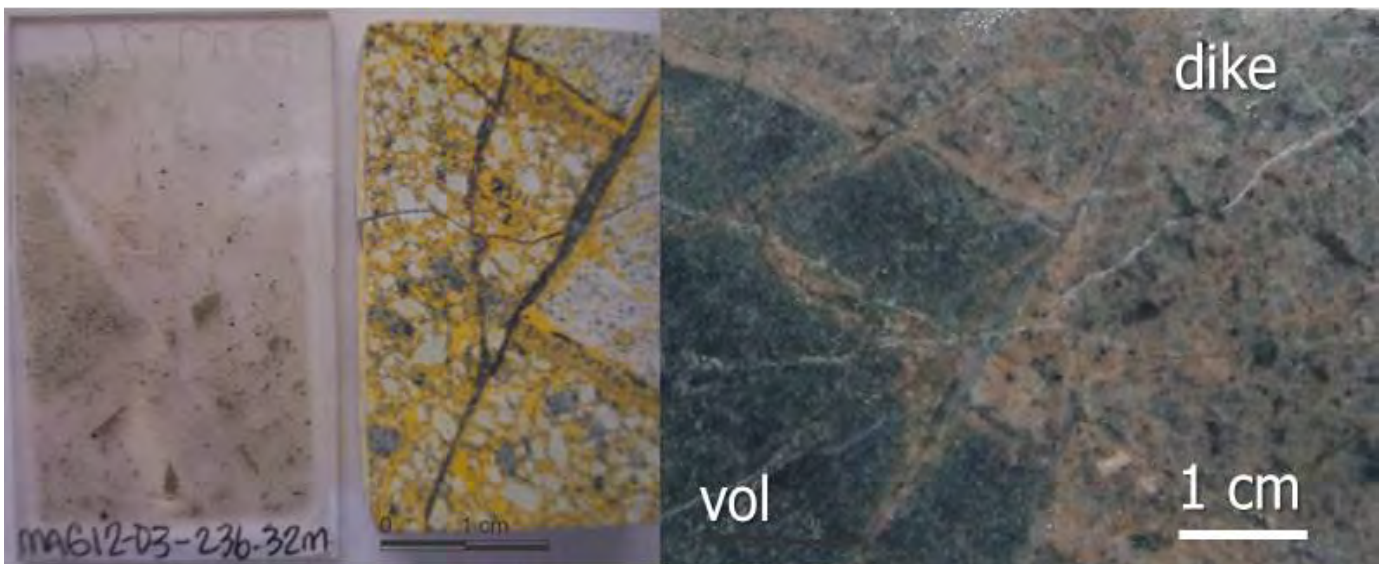


Fig. 13. Syn-mineralization monzonite dike. Thin section (left), stained off-cut (centre) and hand sample (right) are all taken from MAG12-03, at 236.32 m depth. The monzonite dike (dike) has experienced slight post-emplacement faulting and offset at the contact with volcanic host rock (vol).

4.4.4. Aplite dikes

Aplite dikes, 1 to 9 cm wide, are a late intrusive phase that crosscuts main-stage mineralization and all rock types except post-mineralization quartz monzonite. The dikes are light pink to reddish brown, fine grained, equigranular and consist of anhedral quartz and K-feldspar with rare phenocrysts of subhedral plagioclase (Fig. 14). They display moderate chloritic alteration where in contact with suitable lithologies.

4.5. Olivine-phyric basalt: Chilcotin Group (Miocene)

Several discrete basalt flows, each approximately 5 m thick, cap the Three Firs section. These flows are juxtaposed above the Nicola Group along a high-strain zone interpreted to be a fault. Lacking mineralization and significant hydrothermal alteration, this unit is likely part of the Chilcotin Group (Miocene) such as exposed west of the Three Firs prospect (Panteleyev et al., 1996). Vesicle shape, distribution, and orientation indicate that these rocks are upright (Fig. 15). The basalt contains approximately 30% olivine phenocrysts (2 to 3 mm long) and approximately 5% augite phenocrysts (1 mm maximum length) in a very fine-grained groundmass consisting of glass, plagioclase, and minor augite.

5. Three Firs veins, alteration, and mineralization

5.1. Vein paragenesis

Veins at Three Firs veins are divided into eight stages, based on mineral assemblages, textures and crosscutting relationships. We group these veins types into early, main, late and post-mineralization stages based on the presence or absence of Cu and/or Au (Fig. 16).

5.1.1. Early stage pre-mineralization veins: Stages 1 and 2

Stage 1 veins record the earliest hydrothermal fluid event. They are principally adjacent to mineralized dikes in discrete zones of strong potassic alteration. The veins or veinlets consist of magnetite, and are surrounded by very fine-grained K-feldspar alteration envelopes. These veins define the earliest stage of potassic alteration but are unmineralized (Figs. 17a-d). Magnetite veins are typically 1 to 3 mm wide, but rare examples are up to 7 mm wide. Vein margins tend to be diffuse and irregular. Magnetite veins occur singly or, more commonly, in sheeted arrays. They correspond to the early "M" veins developed in many calc-alkaline porphyry Cu-Au deposits as described by Sillitoe (2010).

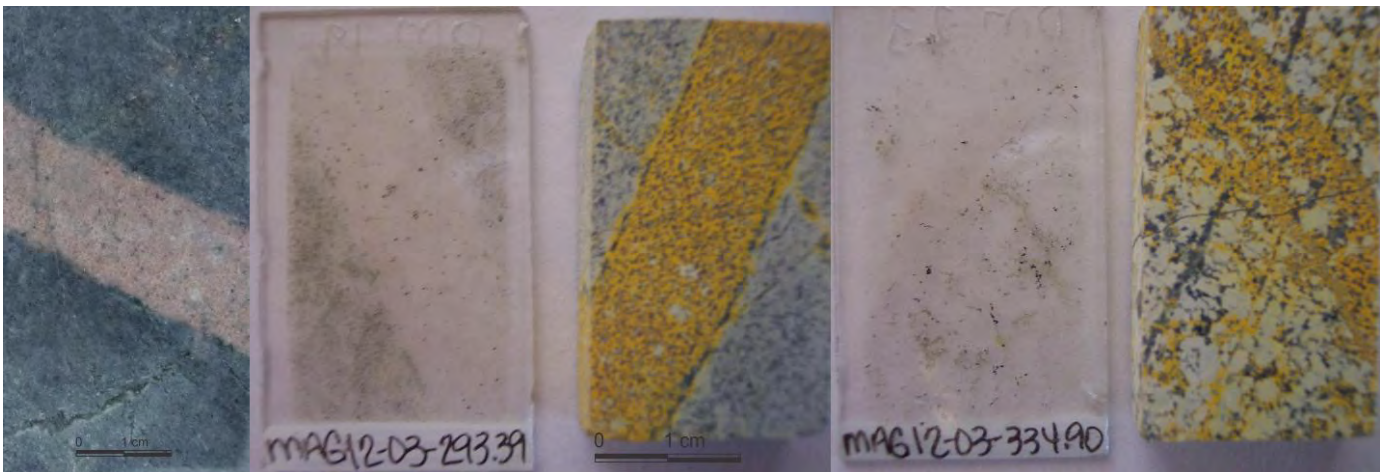


Fig. 14. Aplite dikes. Hand sample (left), thin section (left centre), and stained off-cut (centre) are from MAG12-03 at 293.39 m depth illustrate aplite intruding volcanic sandstone. Thin section (right centre) and stained off-cut (right) are from MAG12-03 at 334.90 m depth illustrate aplite intruding quartz-biotite monzonite.

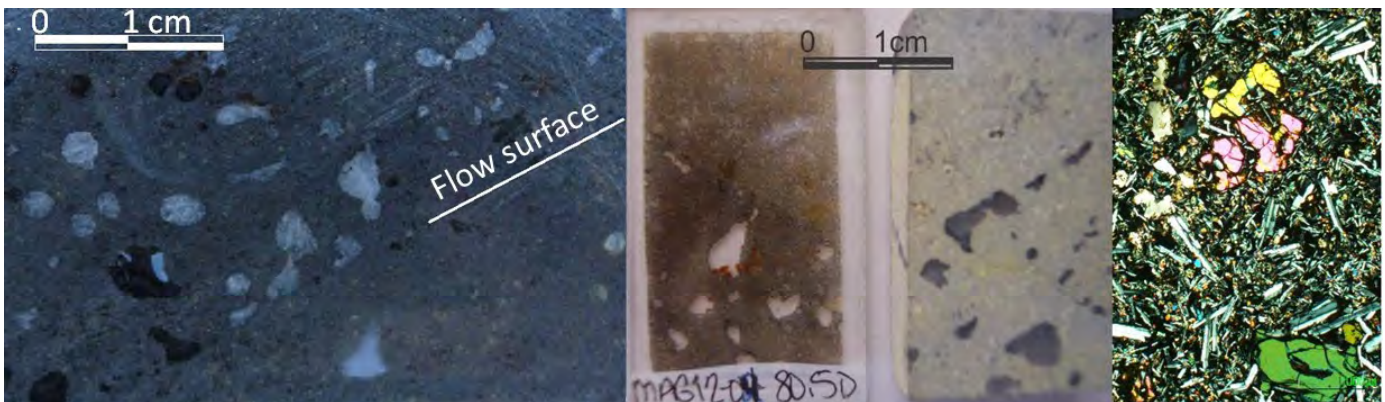


Fig. 15. Olivine-phyric basalt. Hand sample (left) indicating flow surface; thin section (left centre), stained off-cut (right centre) and photomicrograph (right) are all taken from MAG12-04 at 80.50 m depth.

	Vein	Early	Main	Late	Post-min
1	Mag (Early potassic alteration)				
2	Hbl±act±kf (Early calc-potassic alteration)				
3	Qtz-hbl-ccp-py±(bn-cu-cv-cc)±mag±carb±ep±chl±kf (Calc-potassic alteration)				
4	Qtz-(musc-ccp-py±(bn-cu-cv-cc)±hbl±ep±chl±carb±mag (Calc-potassic alteration)				
5	Ccp-py±(bn±cu±cv±cc)±qtz (Phyllic/sericitic alteration)				
6	Qtz-carb-ccp-py±ep±chl±sp (Phyllic/sericitic alteration)				
7	Qtz-py±ccp±carb±tur±ep±chl (Propylitic alteration)				
8	Carb				

Fig. 16. Three Firs vein paragenesis. Line thickness denotes relative abundance of mineral. Only major alteration types are identified for each stage. Abbreviations: Mag-magnetite; Hbl-hornblende; Qtz-quartz; Ccp-chalcopyrite; Py-Pyrite; Bn-bornite; Cu-cubanite; Cv-covellite; Cc-chalcocite; Kf-potassium feldspar; Ep-epidote; Chl-chlorite; Carb-carbonate; Sp-sphalerite; Tur-tourmaline; Musc-muscovite.

Stage 2 veins cut stage 1 veins and consist only of hornblende. In some veins, hornblende is replaced by actinolite. Hornblende veins are present in all Nicola Group lithologies and the pre-mineralization monzonite dikes. In most cases, stage 2 veins are associated with fine-grained K-feldspar halos, which define another early stage of potassic alteration, similar to the stage 1 magnetite veins. Hornblende veins are commonly 1 to 4 mm wide and display diffuse margins. They typically occur singly, but rare sheeted arrays and multi-dimensional stockworks are recognized (Figs. 17 e-h). Epidote replacement of minerals along hornblende vein margins is widespread, but textures suggest that this epidote was not in equilibrium with hornblende. It is likely the result of a later fluid event.

5.1.2. Main stage mineralized veins: Stages 3, 4, and 5

Stage 3 veins crosscut the unmineralized early stage veins and are present in all Nicola Group rocks and pre-mineralization monzonite. Stage 3 veins have diffuse, sinuous margins with minerals only rarely displaying symmetrical distribution as wall-rock parallel bands about a medial suture line. Veins occur singly, in multi-dimensional stockworks or, rarely, as sheeted arrays. Stage 3 veins are 2 - 30 mm wide and consist mainly of

quartz (25-75%), hornblende (20-50%), chalcopyrite (2-15%), pyrite (5-30%), and magnetite (5-50%), with lesser bornite (0-5%) carbonate (0-5%), epidote (0-5%), chlorite (0-5%) and K-feldspar (0-1%) (Fig. 18). Mineralogical variation correlates weakly with host rock composition. For example, veins in the Nicola Group have higher magnetite abundances than those hosted by felsic intrusive rocks.

In diamond-drill holes MAG12-03 and MAG12-05, stage 3 veins contain greater amounts of bornite than chalcopyrite from 360 to 375 m and from 249 to 265 m, respectively. The zones with predominantly bornite also contain native Au in larger grains of disseminated chalcopyrite ± bornite (Fig. 19).

Supergene sulphide minerals replacing chalcopyrite include covellite, cubanite and chalcocite. In some veins, chlorite replaces hornblende. Stage 3 veins have weak to well developed alteration envelopes that reflect, in part, the mineralogy of the host-rock. Envelopes include: 1) fine-grained K-feldspar and rare biotite (potassic alteration assemblage); and 2) sericite-quartz-pyrite with lesser epidote-chlorite (phyllic/sericitic and propylitic alteration assemblages) and rarely albite. Stage 3 veins are comparable to early "A" type veins using the terminology of Gustafson and Hunt (1975).

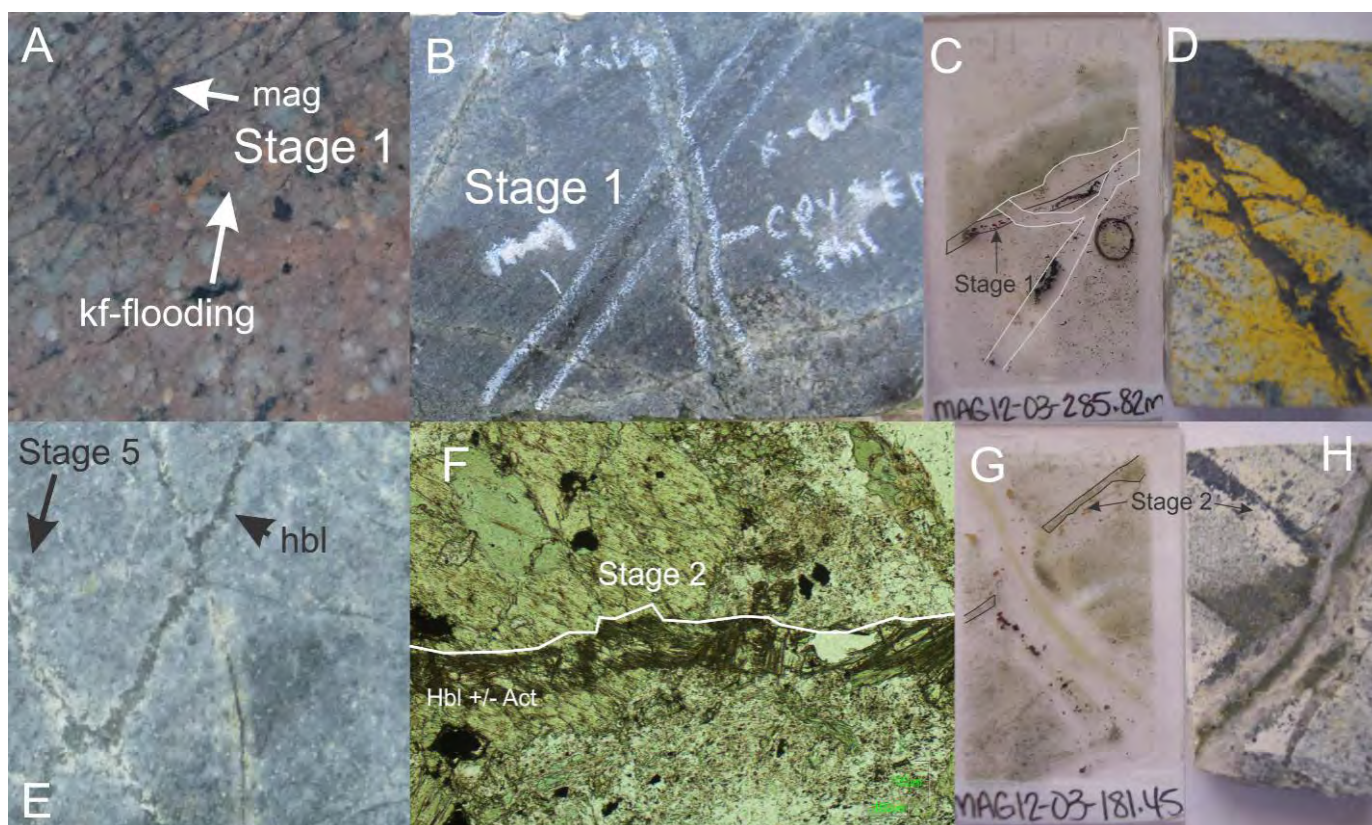


Fig. 17. Hand sample and thin section photomicrographs for Early stage veins. **a)** Hand sample of sheeted magnetite (mag) stringer veinlets. **b)** Individual magnetite vein crosscut by stage 3 vein. **c)** Thin section and **d)** stained off-cut of magnetite veinlet being cross-cut by stage 3 veins. **e)** Hand sample of hornblende (hbl) vein cross cut by stage 5 veinlet. **f)** Thin section photomicrograph of hornblende vein displaying discrete actinolite replacement. **g)** Thin section and **h)** stained off-cut of stage 2 vein crosscut by stage 3 vein.

Stage 4 veins crosscut early stage veins, stage 3 veins, and all pre-mineralization lithologies. They exhibit sharp, straight vein margins, are 3 to 35 mm wide, and have thin medial suture lines filled with chalcopyrite and epidote (Fig. 20). Stage 4 veins consist predominantly of quartz (20-80%) with lesser chalcopyrite (2-15%), pyrite (2-15%), hornblende (0-20%), epidote (0-20%), chlorite (0-10%), carbonate (0-20%) and magnetite (0-10%). These veins occur individually, in stockworks, and as sheeted arrays. Similar to stage 3 veins, bornite is more abundant than chalcopyrite from 360 to 375 m in diamond-drill hole MAG12-03 and from 249 to 265 m in MAG12-05. Supergene sulphide minerals are the same as in stage 3 veins as are the alteration envelopes. They differ from stage 3 veins principally by their sharp vein margins, medial suture lines with epidote and chalcopyrite, much less hornblende, and weaker potassic alteration. Interestingly, chalcopyrite grains display equilibrium textures with hydrothermal epidote implying a direct relation to the Cu-Au mineralization event(s). Stage 4 veins could be classified as “B” veins using the terminology of Gustafson and Hunt (1975).

Stage 5 veins crosscut early stage veins (stages 1 and 2) and, in most cases, main-stage 3 and 4 veins. Stage 5 veins occur in all pre-mineralization lithologies and may be better described as veinlets or “stringer” veins because they are typically less than 2 mm wide, although rare examples are up to 6 mm wide (Fig. 21). Veins have diffuse margins and consist primarily of chalcopyrite, bornite, pyrite, and minor quartz. Chalcopyrite is

locally replaced by supergene cubanite, covellite, and chalcocite. Minor sericite or, more rarely, epidote-chlorite-calcite form alteration halos. These halos do not appear directly related to the hypogene sulphide minerals and may record late ingress of fluids into the pre-existing sulphide veinlets. In common with all previous stages of vein formation, bornite is more abundant than chalcopyrite from 360 to 375 m in MAG12-03 and from 249 to 265 m in MAG12-05. Stage 5 veins normally occur singly or in random stockworks; sheeted arrays are rare. Veins are locally abundant, with up to twenty veins per metre of core. High-density zones and low-density zones of veining alternate but the cause is uncertain. The alternation may be the result of pre-existing structures rather than changes in lithology. Stage 5 veins are comparable to “D” veins or stringer sulphide veins in porphyry deposits using the terminology of Gustafson and Hunt (1975).

5.1.3. Late stage mineralized veins: Stages 6 and 7

Stage 6 veins crosscut stage 5 veins and are found in all lithologies. These veins are 7 to 90 mm wide and typically display exhibit sharp, straight, margins (Fig. 22a). Stage 6 veins display open space-filling textures including comb (Fig. 22b) and rare coliform styles. The veins contain mainly quartz (30-75%), carbonate (20-80%) and, in some cases, sphalerite (0-50%). Chalcopyrite (0-5%), pyrite (0-50%), epidote (0-10%), chlorite (0-10%) and tetrahedrite/tennantite (0-5%) are minor phases. Stage 6 veins are uncommon in the Three Firs prospect



Fig. 18. Hand sample of fragmented stage 3 quartz vein with magnetite-rich margins.

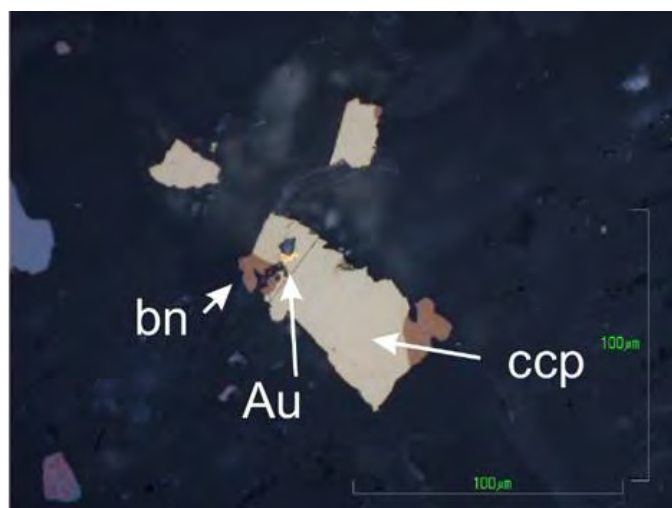


Fig. 19. Photomicrograph of native gold (Au) in chalcopyrite-bornite (ccp-bn) dissemination from MAG12-03 at 363.71 m.

but where present, correlate weakly with pre-mineralization quartz-biotite monzonite dikes. They produce strong carbonate

alteration halos and weaker sericite-chlorite (phyllic) alteration. These late stage carbonate-base metal veins are common in large porphyry systems (e.g., Corbett and Leach, 1998).

Stage 7 veins crosscut those of stage 5, but have variable crosscutting relationships with those of stage 6. They exhibit a range of textures, mineral modes, and widths (Fig. 23). They consist of quartz (20-90%), pyrite (2-50%), chalcopyrite (0-5%) carbonate (0-50%), epidote (0-50%), chlorite (0-50%), and tourmaline (0-75%). Stage 7 veins occur singly or, more rarely, in discrete arrays. Vein margins range from sharp and straight to irregular and diffuse. Diffuse margins tend to correlate with higher tourmaline abundances. Adjacent to stage 7 veins are zones of propylitic alteration consisting of epidote, chlorite, and calcite; these zones do not correlate with strong Cu-Au mineralization.

5.1.4. Post-mineralization veins: Stage 8 veins

Stage 8 veins are unrelated to Cu-Au mineralization and post-date all stages of vein formation. They consist of calcite with lesser ankerite as indicated by surface staining and reflectance spectroscopy (Fig. 24a and see below). With sharp and irregular margins, the veins form singly or in swarms with multiple bifurcations (Fig. 24b). Host-rocks display minor calcite alteration adjacent to the veins.

5.2. Prospect-scale alteration

Rocks hosting the Three Firs prospect are pervasively altered and display evidence of superimposed alteration events. Common alteration assemblages include potassic, calc-potassic, phyllic (sericitic), and propylitic. The formation of these assemblages can be attributed directly to different stages of vein formation. Although we lack data to rigorously define the spatial distribution of vein types and alteration throughout the property, graphical logs and thin section petrography derived from drill holes allow us to identify the general mineralogical and textural characteristics of the alteration assemblages

5.2.1. Potassic and calc-potassic alteration

Early potassic alteration is spatially associated with stage 1, 2, and 3 veins and, to a lesser extent, with stage 4 and 5 veins. It is expressed in two styles: 1) predominantly K-feldspar (K-feldspar ± magnetite ± sericite ± biotite ± chalcopyrite-pyrite ± bornite) adjacent to vein margins as alteration envelopes; and 2) predominantly biotite-magnetite (biotite-magnetite ± sericite ± K-feldspar ± chalcopyrite-pyrite ± bornite) as dark brown patches throughout the Nicola Group. Magnetite is not a distinguishing feature of potassic alteration because it is pervasively distributed throughout Nicola Group rocks as both a primary igneous mineral and a product of secondary hydrothermal alteration.

Calc-potassic alteration is characterized by hornblende-actinolite-K-feldspar-epidote ± titanite ± chalcopyrite ± bornite. It probably represents a transitional potassic alteration assemblage resulting from variations in host-rock composition rather than a discrete calc-potassic hydrothermal fluid event.

5.2.2. Phyllic (sericitic) alteration

Phyllic alteration is characterized by both microscopic sericite and medium-grained flaky “sericite” (identified as muscovite in hand sample). In practice, the term “phyllic” is

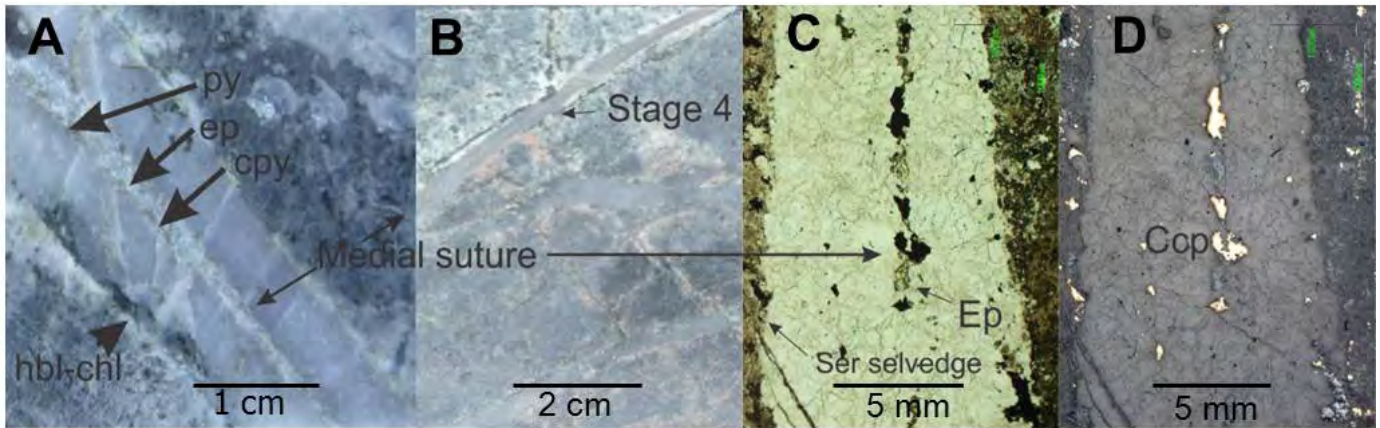


Fig. 20. Hand sample and photomicrographs of stage 4 veins with characteristic medial sutures. **a)** and **b)** are hand samples. **c)** and **d)** are transmitted and reflected light photomicrographs from thin sections of the vein in **b)**. Abbreviations as in Figure 16.

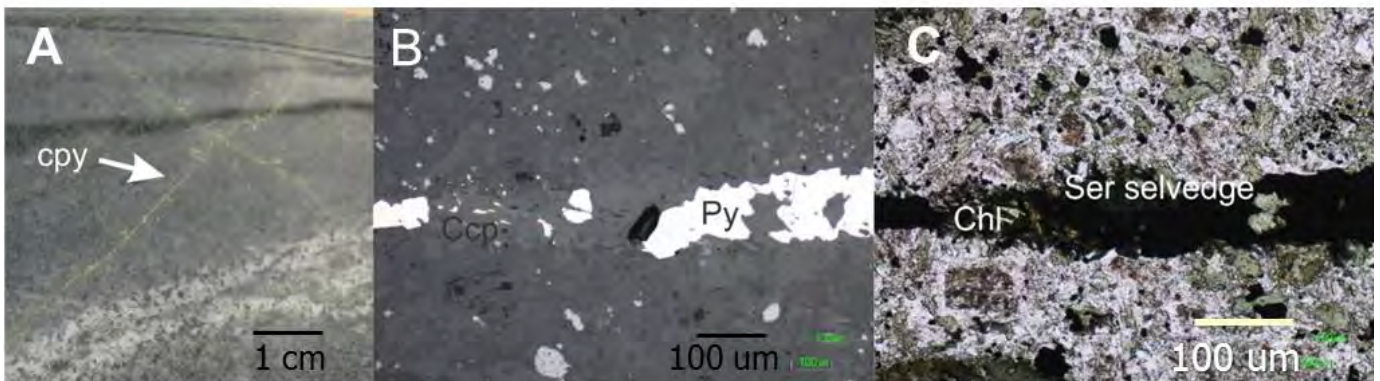


Fig. 21. **a)** Hand sample of stage 5 chalcopyrite-pyrite-quartz stringer vein. **b)** Reflected light and, **c)** transmitted light photomicrographs of chalcopyrite-pyrite-quartz stringer vein in thin section.

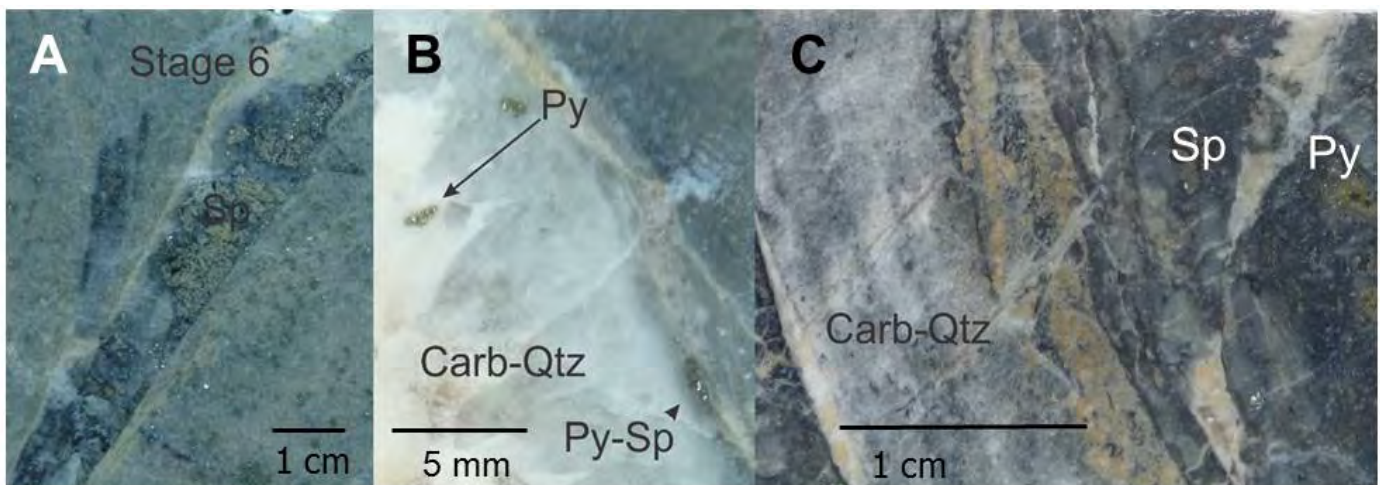


Fig. 22. Hand samples of Late stage 6 veins. **a)** Stage 6 vein with pale grey sericite and carbonate alteration. **b)** Comb-textured quartz crystals growing perpendicular to the vein wall margin. **c)** Laminated stage 6 vein with parallel mineral layers of carbonate, quartz, and grey sulphides (tetrahedrite, sphalerite, chalcopyrite and pyrite). Abbreviations as in Figure 16.

used rather than sericite or muscovite because the true variety of white mica is uncertain (e.g., Beane and Titley, 1981). Phyllic alteration forms halos around stage 5 and 6 veins. It also pervasively alters rock in narrow faults and shear zones.

These structures produce highly fragmented zones in drill core. Phyllic alteration post-dates potassic alteration throughout the Three Firs prospect, and typically consists of quartz-sericite-pyrite ± chlorite ± epidote ± calcite in various combinations. It

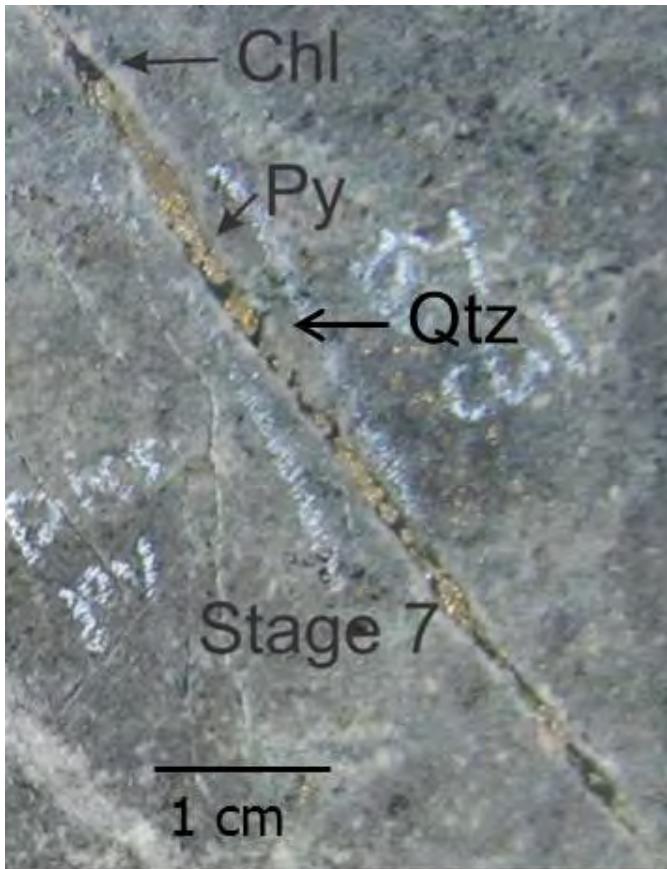


Fig. 23. a) Stage 7 vein with quartz (Qtz) and lesser pyrite (Py); propylitic alteration with predominantly chlorite (Chl) and epidote.

is associated with hypogene covellite, chalcocite, cubanite, and bornite. Reflectance spectroscopic analysis of phyllic alteration halos around stage 5 veins (see below) identified crystalline illite and hydromuscovite (Fig. 25). Phyllic alteration in the currently known Three Firs system is weak compared to other large calc-alkaline porphyry Cu deposits in British Columbia such as Kemess South (Duuring et al., 2009a) and Highland

Valley (McMillan, 2005).

5.2.3. Propylitic alteration

Propylitic alteration is ubiquitous throughout the Three Firs prospect and locally replaces potassic and phyllic alteration assemblages. Mineralogy varies, but consists of epidote-calcite-chlorite \pm pyrite \pm minor albite. Host rock hornblende, plagioclase, and alkali feldspar are selectively replaced. Late stage 7 veins are commonly associated with propylitic alteration.

6. Three Firs whole-rock geochemistry

Twenty-one samples of the least altered rock types were selected for whole-rock geochemical analysis using existing pulps from the four MAG12 drill cores.

6.1. Geochemical methods

Samples were analyzed using ME-ICP06 (inductively coupled plasma) and OA-GRA05 methods. Major oxides were analyzed by ICP-AES (atomic emission spectroscopy) at ALS Laboratories Limited. Samples were decomposed by lithium metaborate/lithium tetraborate ($\text{LiBO}_2/\text{Li}_2\text{B}_4\text{O}_7$) fusion (FUS-LI01). The procedure for ME-ICP06 analysis used 0.2 g of sample (pulverized) mixed with 0.90 g lithium metaborate/lithium tetraborate flux that underwent fusion at 1000° C. The cooled melt was dissolved in 100 ml of 4% nitric acid and 2% hydrochloric acid, and analyzed by ICP-AES. Elemental concentrations were used to determine oxide concentration values. In the accompanying OA-GRA05 method, ICP analyte concentrations and loss-on-ignition (L.O.I.) values were used to determine the total oxide content, where percent L.O.I. was calculated from the weight difference after 0.1 g sample was placed in a 1000° C oven for one hour.

ME-MS81 is an ultra-trace level method that is used for whole rock samples. Lithium metaborate fusion (FUS-LI01) decomposed the sample and products were then analyzed by Inductively Coupled Plasma Mass Spectrometry (ICP-MS). A 0.2 g sample was mixed with 0.9 g lithium metaborate and fused at 1000° C. The cooled melt was dissolved in 100 ml of 4% nitric acid and 2% hydrochloric acid and analyzed by

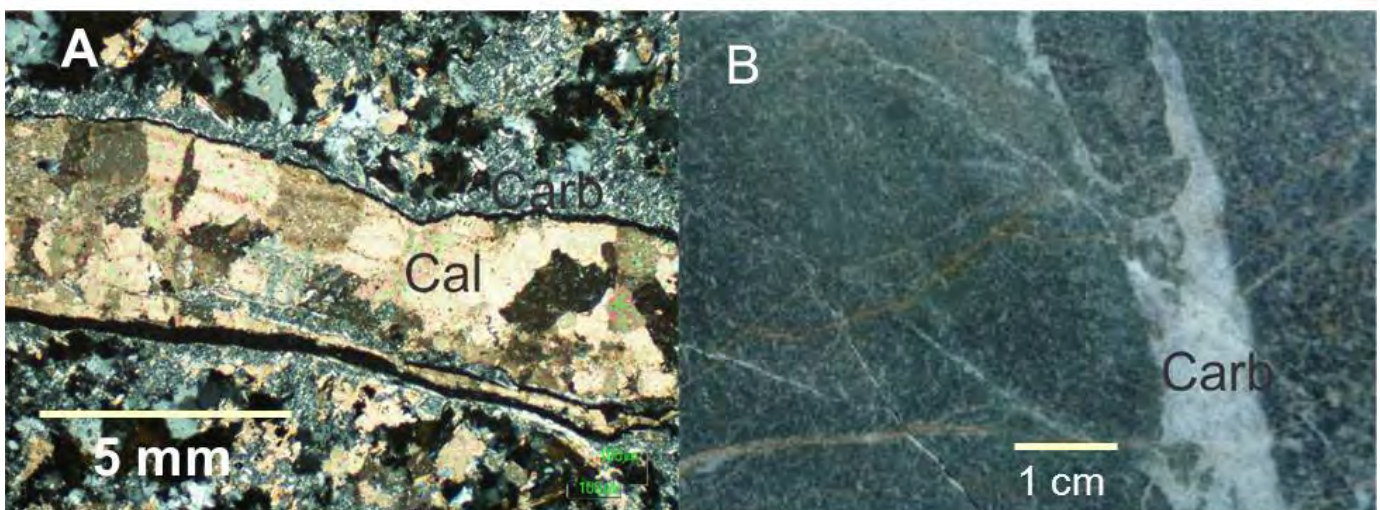


Fig. 24. Stage 8 carbonate veins. a) Photomicrograph (crossed-polarized light) of calcite vein and **b)** hand sample displaying irregular vein margins and multiple bifurcations.

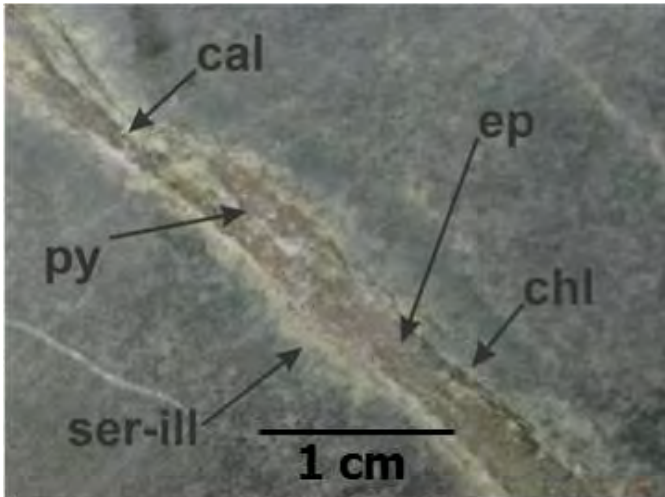


Fig. 25. Phyllic alteration halos around stage 5 veins with crystalline illite and hydromuscovite identified by reflectance spectroscopy.

ICP-MS.

Gold values were determined by AU-ICP21 with a fire assay fusion ICP-AES finish. Each sample was fused with a mixture of lead oxide, sodium carbonate, borax and silica. This combination was inquarted with 6 mg of gold-free silver and cupelled to produce a metal bead. The bead was then digested in 0.5 ml of dilute nitric acid and 15 ml of hydrochloric acid in a microwave oven. The resulting cooled solution was diluted with 4 ml of demineralized water and analyzed by ICP-AES against matrix-matched standards. Complete details on the analytical methodology and quality assurance/quality control (QA/QC) are given in Sherlock et al. (2013).

6.2. Whole-rock geochemistry results

Most drill core samples exhibit strong alteration, as expected in rocks near a large hydrothermal system. Consequently, although considerable care was taken to select sample intervals that had minimal visible alteration, geochemical analyses (Table 1) indicate that only seven samples have L.O.I. values below 3.0 wt.%, the approximate upper limit for unaltered granitic rocks (e.g., Lemaitre, 1978). All other samples have some degree of alteration. On a binary plot of K_2O (wt.%) versus SiO_2 (wt.%), most samples fall in the medium-K calc-alkaline field (Fig. 26). The few samples that plot in the high-K calc-alkaline field have been affected by secondary potassic alteration (biotite and sericite) as evidenced by relatively high L.O.I. values (Table 1). On the Rb versus Y+Nb tectonic discrimination diagram of Pearce (1984), all samples plot in the field for volcanic arc granites (Fig. 27). This origin is consistent with the generation of Three Firs magmas in the southern Nicola volcanic arc.

7. Fluid inclusion microthermometry of main-stage hydrothermal veins

To estimate the temperature, pressure and compositional conditions of the ore fluids during metal deposition, four doubly-polished 80 μm thick sections from quartz veins were examined, two from each of stages 3 and 4 (Fig. 28). These veins were selected because they host most of the Cu-Au mineralization in the prospect and contain quartz grains that are suitable (i.e. clear and unrecrystallized) for microthermometric

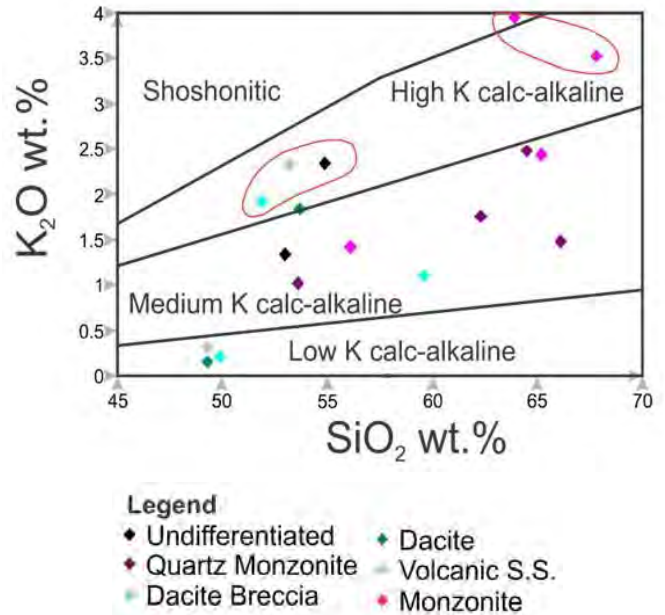


Fig. 26. K_2O vs. SiO_2 (wt.%) diagram (after Peccerillo and Taylor, 1976) for Three Firs samples. Samples circled in red in the high K calc-alkaline field have been affected by secondary potassic alteration (see text for discussion).

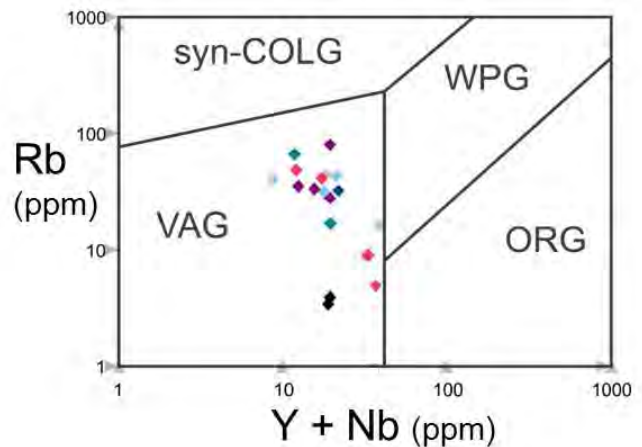


Fig. 27. Trace element tectonic discrimination diagram (after Pearce, 1984) for Three Firs samples.

analysis. These veins are interpreted to be within the central region of the Three Firs porphyry Cu-Au system based on drilling and exploration activities.

Microthermometric analysis was conducted using a Linkam THMSG 600 heating-freezing stage at the British Columbia Geological Survey (BCGS). Accuracy of measurement is $\pm 5^\circ C$ above $200^\circ C$, $\pm 1^\circ C$ between $100^\circ C$ and $200^\circ C$ and $\pm 0.1^\circ C$ below $100^\circ C$.

7.1. Types of fluid inclusions

Fluid Inclusions in hydrothermal quartz are divided into primary, pseudosecondary, and secondary inclusions using the criteria of Roedder (1984) and based on their phase proportions

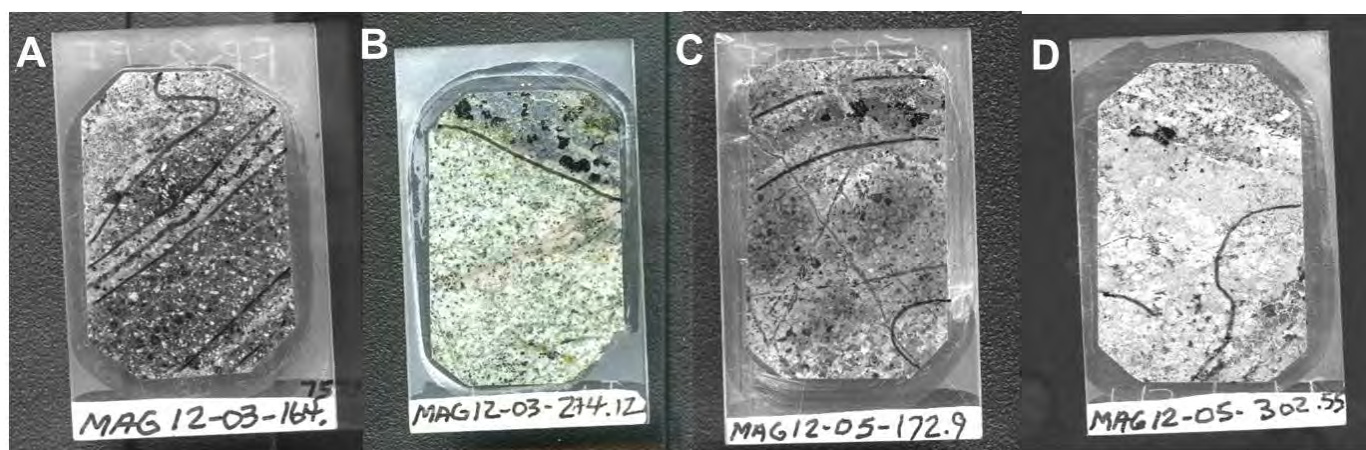


Fig. 28. Doubly polished (80- μm) thin sections of main stage veins studied for fluid inclusion microthermometry. **a)** MAG12-03 (164.75 m), stage 4. **b)** MAG12-03 (274.12 m), stage 3. **c)** MAG12-05 (172.90 m), stage 3. **d)** MAG12-05 (302.55 m), stage 4.

at room temperature (25° C) and behaviour during heating and freezing experiments. Studied fluid inclusions are further subdivided into distinct fluid inclusion assemblages (FIAs) using the criteria of Goldstein and Reynolds (1994). An individual FIA is a group of fluid inclusions that are interpreted to represent coeval inclusions that formed during a single fluid event.

Primary and pseudosecondary fluid inclusions fall into three compositional types at Three Firs (Fig. 29). Type 1 inclusions are aqueous, brine-rich, multiphase (liquid + vapour + halite \pm sylvite \pm carbonate \pm sulphide daughter minerals) inclusions that contain less than 10 vol.% vapour. Type 2 inclusions are aqueous and typically liquid-rich (liquid + vapour \pm carbonate daughter) with 10 to 35 vol.% vapour. Type 3 inclusions are two-phase (vapour + liquid), aqueous and vapour-rich, with greater than 80 vol.% vapour. Secondary fluid inclusions are common in all stages of vein formation and typically occur as two-phase (liquid \pm vapour), liquid-rich inclusions in trails and arrays that crosscut quartz grain boundaries. Their timing with respect to the Cu-Au mineralization is unclear and they are not discussed further. It is assumed that the volume and composition of primary and pseudosecondary inclusions has remained constant after entrapment. In other words, they have not leaked. This assumption is based on the shape of inclusions (no “necks” or “tails”) and characteristics of the host quartz grains. Specifically, grains show uniform extinction in cross-polarized light and lack deformation or recrystallization textures (Roedder, 1984; Goldstein and Reynolds, 1994).

Stage 3 quartz-hornblende \pm magnetite \pm chalcopyrite \pm pyrite veins contain 0.25 to 2.5 mm diameter quartz grains that are unzoned, anhedral, and commonly in contact with primary sulphides. Fluid inclusion assemblages in quartz include numerous trails of secondary inclusions that crosscut grain boundaries, and trails, clusters, and arrays of primary and pseudosecondary FIAs that terminate at grain boundaries (Fig. 29b). Microthermometric measurements were made on the Type 1 brine-rich, Type 2 liquid-rich, and Type 3 vapour-rich inclusions, but only the Type 1 inclusion data are considered reliable (see below). Some Type 1 inclusions contained rare, opaque, triangular daughter minerals identified as chalcopyrite using reflected light microscopy (Fig. 29a). Measured inclusions had irregular, equant, and negative crystal shapes,

and ranged from 5-20 μm in long dimension (mean $8 \pm 3 \mu\text{m}$).

Stage 4 veins contain 0.2 -3.0 mm-diameter quartz grains that are clear, unzoned, and anhedral and contain variable amounts of hornblende \pm magnetite \pm epidote \pm chlorite \pm carbonate \pm K-feldspar \pm sericite and sulphides. Stage 4 veins have sharp, straight margins and medial suture lines. Fluid inclusion assemblages in quartz include secondary, pseudosecondary and primary FIAs. The primary inclusions form discrete clusters and trails that terminate at quartz grain boundaries. Type 1 brine-rich, Type 2 aqueous liquid-rich, and Type 3 vapour-rich varieties are all abundant as primary and pseudosecondary inclusions. Studied inclusions displayed irregular to equant negative crystal shapes that ranged from 5 to 25 μm in long dimension (mean $9 \pm 4 \mu\text{m}$).

7.2. Microthermometric results

7.2.1. Stage 3 veins

Fluid inclusions were cooled to -110° C and reheated slowly to check for CO₂, identify major cations, and calculate fluid salinities where possible. Eutectic (T_e) and final ice melting temperatures (T_m) were not collected from Type 3 vapour-rich inclusions because of the difficulty observing the first (eutectic) and final melting of solid ice. Carbonic fluids were not detected in any of the fluid inclusions studied. The Type 1 FIAs predominately homogenized by halite dissolution (Fig. 30), which indicates that they are not the result of unmixing or “boiling” of a supercritical fluid on the H₂O-NaCl solvus into immiscible vapour and liquid phases (e.g., Bodnar and Vityk, 1994). Salinities calculated using the dissolution temperatures of halite during heating of Type 1 inclusions range from 37.8 to 47.9 equivalent weight percent NaCl (equiv. wt.% NaCl) with a mean of 41.6 equiv. wt.% NaCl (n = 9). The T_e measured during freezing of Type 1 inclusions are below the eutectic temperature for pure NaCl-H₂O (-21.2° C). This implies the presence of dissolved cations other than Na⁺ (e.g., Shepherd et al., 1985). This finding is consistent with the existence of sylvite (KCl) and carbonate daughter minerals (calcite, dolomite, and ankerite) in Type 1 inclusions, which indicate the presence of K⁺, Ca²⁺ Mg²⁺ and Fe^{2+,3+} in addition to Na⁺. The presence of cations other than Na⁺ is the reason that salinity is expressed as “equivalent weight percent NaCl” (e.g., Shepherd et al., 1985). Type 1 brine-rich inclusions have a homogenization

Table 1. Major (wt.%) and trace (ppm) element data. Abbreviations as follows: Dacite BX=plagioclase-hornblende-phyric dacite breccia; Dacite=plagioclase-hornblende-phyric dacite; HBX=hydrothermal breccia; VolSS=volcanic sandstone; Undiff=undifferentiated lithology; Monz=monzonite; Qtz-bio monz=quartz-biotite monzonite; Qtz monz=quartz monzonite.

Lithology	Qtz-bio monz	Dacite BX	Qtz monz	Basalt	Basalt	Dacite BX monz	VolSS	Qtz-bio monz	Qtz-bio monz	Qtz monz	
Hole_ID	MAG12-03	MAG12-03	MAG12-03	MAG12-04	MAG12-04	MAG12-04	MAG12-05	MAG12-05	MAG12-05	MAG12-05	
From (m)	333.6	366	405	78	84	125	229	255	302.55	331	361
To (m)	335	368	406.91	81	86.15	127	231	257	303.27	332.1	363
Au_ppm	0.011	0.155	0.039	0.001	0.002	0.003	0.029	0.045	0.041	0.066	0.005
Cu%	0.0385	0.126	0.21	0.0051	0.0058	0.0276	0.141	0.152	0.0376	0.071	0.0197
SiO2%	67.8	51.9	65.2	49.5	46.8	59.6	66.1	53.2	64.5	62.3	53.6
Al2O3%	14.75	16.6	15.05	14.75	16.2	18.5	15.25	17.05	16.7	17.2	16.95
Fe2O3%	3.32	10.8	2.24	10.75	9.11	3.01	2.38	9.38	4.47	5	8.34
CaO%	3.95	7.45	4.67	10.5	11.2	5.01	4.13	4.36	4.43	4.27	8.61
MgO%	1.09	5.03	0.93	5.21	2.94	2.45	1.27	5.01	1.55	1.96	4.12
Na2O%	3.74	3.73	2.54	3.28	3.31	4.12	3.57	2.82	4.33	4.38	3.63
K2O%	3.53	1.92	2.44	0.61	0.45	1.11	1.48	2.33	2.48	1.76	1.02
Cr2O3%	-0.01	0.01	-0.01	0.04	0.05	-0.01	-0.01	-0.01	-0.01	-0.01	0.01
TiO2%	0.32	0.84	0.33	1.75	1.97	0.54	0.36	0.7	0.43	0.5	0.75
MnO%	0.04	0.14	0.16	0.24	0.35	0.09	0.06	0.1	0.03	0.03	0.1
P2O5%	0.12	0.25	0.12	0.3	0.38	0.27	0.14	0.29	0.19	0.21	0.24
SrO%	0.06	0.07	0.03	0.09	0.12	0.05	0.04	0.06	0.09	0.09	0.07
BaO%	0.2	0.09	0.12	0.05	0.04	0.02	0.03	0.06	0.21	0.17	0.05
LOI%	1.72	2.9	6.43	4.12	5.65	5.85	4.5	4.54	1.71	2.44	3.56
Total%	100.64	101.73	100.26	101.19	98.57	100.62	99.31	99.9	101.12	100.31	101.05
Ag_ppm	-1	-1	1	-1	-1	-1	1	-1	-1	-1	-1
Ba_ppm	1670	728	969	388	343	153	276	509	1670	1370	404
Ce_ppm	7.7	15.3	17.5	25.7	28	14.3	9.4	18.5	15.3	19.9	14.1
Co_ppm	6.4	21.7	4	49.2	43.2	18	19.4	21.5	7.4	11.1	18.1
Cr_ppm	30	80	30	340	360	20	30	20	30	30	60
Cs_ppm	0.42	1.14	5.08	0.28	0.13	2.46	2.29	2.71	0.79	1.14	1.17
Cu_ppm	327	1150	1865	51	57	264	1325	1405	359	659	220
Dy_ppm	1.13	3.55	1.7	3.95	4.38	2.57	1.5	3.2	1.72	2.19	3.05
Er_ppm	0.7	2.07	1.06	1.9	2.07	1.66	0.97	1.86	1	1.3	1.78
Eu_ppm	0.53	0.97	0.62	1.61	1.77	0.71	0.51	0.81	0.74	0.86	0.94
Ga_ppm	16.7	18.2	16.6	21.3	22.9	18.7	16.2	18.2	18.9	21	19.5
Gd_ppm	1.13	3.34	1.79	4.63	5.11	2.3	1.47	2.93	1.87	2.44	3.09
Hf_ppm	2.9	1.6	3	3.1	3.2	2	3.1	2	3.2	2.9	2
Ho_ppm	0.24	0.74	0.36	0.76	0.83	0.58	0.33	0.67	0.35	0.48	0.67
La_ppm	3.9	6.9	9.1	12.1	13.1	7.5	4.7	8.9	7.8	9.6	6.5
Lu_ppm	0.14	0.32	0.2	0.23	0.25	0.31	0.19	0.3	0.17	0.24	0.3
Mo_ppm	3	2	2	2	2	7	3	-2	2	2	6
Nb_ppm	1.7	1.5	3.1	13.8	15.3	1.9	2.5	1.7	2.4	2.8	1.6
Nd_ppm	4.5	10.7	8.6	16	17.3	8.4	5.5	11.3	8.3	10.9	9.4
Ni_ppm	8	23	6	185	127	7	10	12	9	9	20
Pb_ppm	5	5	5	-5	-5	9	-5	8	5	-5	-5
Pr_ppm	1.03	2.25	2.25	3.51	3.87	1.92	1.3	2.48	1.98	2.63	2.04
Rb_ppm	40.3	43	79.1	8.9	4.9	41.2	48.1	79.4	34.8	33.3	27.8
Sm_ppm	1.04	2.66	1.89	4.45	4.59	2.04	1.33	2.76	1.9	2.54	2.6
Sn_ppm	1	1	1	1	1	1	1	1	1	2	1
Sr_ppm	524	541	274	751	1015	369	311	453	697	701	568
Ta_ppm	0.2	0.1	0.3	0.9	1.1	0.1	0.2	0.1	0.2	0.2	0.1
Th_ppm	3.86	0.99	5.08	1.72	1.55	1.09	3.81	1.22	3.06	2.58	1.31
Tl_ppm	-0.5	-0.5	-0.5	-0.5	-0.5	-0.5	-0.5	-0.5	-0.5	-0.5	-0.5

Table 1. Cont'd.

Lithology	Dacite BX	Dacite	HBX	VolSS	Undiff	Basalt	Undiff	Monz	Qtz-bio monz	Dacite
Hole_ID	MAG12-02	MAG12-02	MAG12-02	MAG12-02	MAG12-02	MAG12-03	MAG12-03	MAG12-03	MAG12-03	MAG12-03
From (m)	48	122	157.93	189	308	106.68	226.89	235.28	293	309
To (m)	51	123.68	160.37	192	310.29	109	228	237	295	311
Au_ppm	0.001	0.003	0.247	0.006	0.017	0.002	0.15	1.215	0.077	0.062
Cu%	0.0029	0.0134	0.19	0.0135	0.0339	0.0089	0.216	0.741	0.125	0.0811
SiO2%	49.9	49.3	54.9	49.3	53	49.2	56.1	63.9	54.1	53.7
Al2O3%	17.55	16.9	10.25	17.4	17.4	14.05	15.85	14.35	17.55	17.05
Fe2O3%	9.84	11.65	10.95	9.37	9.54	11.05	6.85	4.25	8.3	8.94
CaO%	7.95	8.76	6.63	8.03	7.68	9.02	6.86	3.81	7.92	8.13
MgO%	3.84	4.43	1.05	4.25	4.15	7.33	2.74	1.19	3.82	3.9
Na2O%	4.06	4.07	0.22	3.58	3.53	3.12	3.56	2.57	4.67	4.16
K2O%	0.21	0.15	2.34	0.32	1.34	0.96	1.42	3.95	1	1.84
Cr2O3%	-0.01	-0.01	-0.01	-0.01	-0.01	0.04	-0.01	-0.01	-0.01	-0.01
TiO2%	0.79	0.82	0.49	0.72	0.77	1.79	0.59	0.37	0.68	0.67
MnO%	0.08	0.11	2.57	0.1	0.36	0.13	0.12	0.14	0.11	0.13
P2O5%	0.24	0.18	0.13	0.23	0.32	0.37	0.26	0.22	0.25	0.2
SrO%	0.07	0.07	0.01	0.13	0.09	0.08	0.05	0.04	0.07	0.06
BaO%	0.02	0.01	0.02	0.02	0.08	0.05	0.05	0.21	0.05	0.08
LOI%	5.86	2.77	9.15	5.46	3.7	3.12	3.87	3.54	2.96	2.34
Total%	100.41	99.22	98.71	98.91	101.96	100.31	98.32	98.54	101.48	101.2
Ag_ppm	-1	-1	62	-1	-1	-1	1	4	-1	-1
Ba_ppm	193	102	174.5	165.5	626	383	453	1670	377	613
Ce_ppm	17.5	10.3	8.2	8.9	18.6	33.5	17	11.9	14.9	12.9
Co_ppm	14.9	24.8	70.9	15.4	24.6	42.4	12.3	12.5	20.3	20.1
Cr_ppm	20	30	30	20	20	310	20	20	30	40
Cs_ppm	1.86	1.31	5.35	1.13	1.16	0.21	2.68	2.63	0.9	0.63
Cu_ppm	28	127	1805	127	341	76	2040	5880	1120	708
Dy_ppm	3.27	3.18	1.79	2.95	3.55	4.06	2.85	1.67	3.06	2.74
Er_ppm	2.02	1.95	1.08	1.78	2.25	1.99	1.73	1.03	1.85	1.67
Eu_ppm	1.11	0.79	0.44	0.69	0.99	1.63	0.84	0.56	0.84	0.72
Ga_ppm	19.9	18.5	12.8	19.1	19.4	22	17.7	15.1	19.3	18.7
Gd_ppm	3.15	2.97	1.6	2.61	3.39	4.97	2.72	1.7	2.88	2.65
Hf_ppm	1.4	1.3	0.9	1.3	1.7	3.1	1.8	2.5	1.6	1.5
Ho_ppm	0.66	0.65	0.37	0.59	0.72	0.73	0.61	0.34	0.63	0.58
La_ppm	7.8	4.4	3.6	3.7	8.4	15.4	8.4	5.4	6.7	5.6
Lu_ppm	0.27	0.26	0.16	0.26	0.32	0.23	0.27	0.18	0.3	0.28
Mo_ppm	-2	4	374	6	2	3	3	4	4	3
Nb_ppm	1.3	1.2	1	1.3	1.7	18.5	1.9	1.8	1.9	1.7
Nd_ppm	9.7	7.2	5.1	6.6	11.3	19.2	10.5	7	9.9	8.7
Ni_ppm	11	13	22	7	12	107	10	7	13	14
Pb_ppm	-5	5	582	10	6	19	18	90	5	5
Pr_ppm	2.26	1.48	1.11	1.3	2.57	4.43	2.41	1.61	2.18	1.9
Rb_ppm	3.9	3.4	90.7	11.2	32	16.4	43.8	65.9	16.8	31.3
Sm_ppm	2.59	2.24	1.36	1.98	2.85	4.75	2.59	1.61	2.53	2.23

(to the liquid phase) temperatures (T_h) that range from 210 to 302° C. Total homogenization temperatures (T_h total) indicated by the dissolution of halite range from 295 to 404° C (Table 2). Individual FIAs show < 15° C variation between T_h .

7.2.2. Stage 4 veins

Similar to stage 3 veins, all fluid inclusions were cooled to -110° C and slowly reheated to check for CO₂, identify the major cations, and to calculate salinities where possible.

Carbonic fluids were not detected in any of the fluid inclusions. Eutectic temperatures and final ice melting temperatures were not collected in Type 3 vapour-rich inclusions owing to the difficulty observing the first and final melting of solid ice. The Type 1 FIAs display predominantly halite-homogenization characteristics (Fig. 30). Salinities calculated using the dissolution temperatures of halite during heating range from 34.7 to 49.7 equiv. wt.% NaCl (mean = 41.7 equiv. wt.% NaCl, n = 7). The eutectic temperatures measured during freezing of

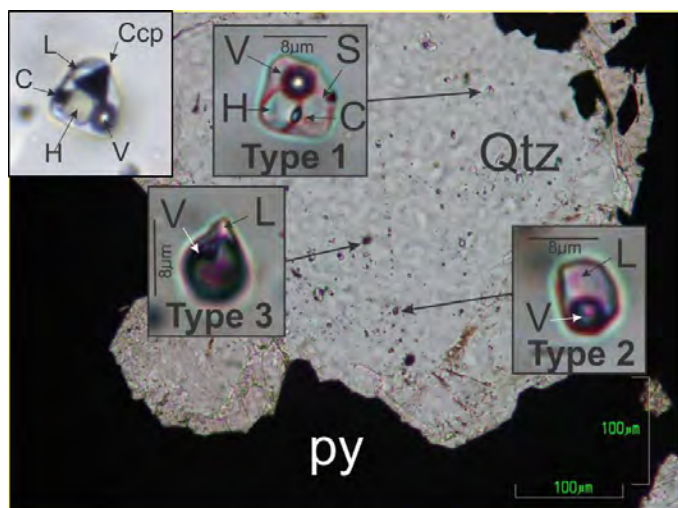


Fig. 29. Fluid inclusion classification at Three Firs. **a)** Photomicrographs of hydrothermal quartz adjacent to pyrite containing: Type 1 halite-saturated, multisoild, aqueous, liquid-rich inclusions; Type 2 “mixed” aqueous, liquid-rich inclusions; and Type 3 low salinity, aqueous, vapour-rich inclusions. Note the opaque, triangular chalcopyrite (Ccp) daughter mineral in Type 1 inclusion in top left inset figure. **b)** Type 1 FIAs occurring as primary clusters and in pseudosecondary trails in hydrothermal quartz. Abbreviations: L=liquid, V=vapour, H=halite, C=carbonate, Ccp=chalcopyrite, Py=pyrite, Qtz=quartz.

Type 1 inclusions are below the eutectic for pure NaCl-H₂O (-21.2° C), which indicate the presence of K⁺, Ca²⁺ Mg²⁺ and Fe^{2,3+} in addition to Na⁺ (Shepherd et al. 1985). Type 1 brine-rich inclusions have T_h (to the liquid phase) that range from 237 to 430° C and (T_h total), indicated by the dissolution of the halite daughter crystal, that range from 250 to 420° C (Table 2). Individual FIAs have < 15° C variation between T_h.

7.3. Physiochemical conditions of the hydrothermal ore fluids at Three Firs

In both stage 3 and 4 veins, Type 1 inclusions homogenized by halite dissolution at temperatures higher than those recorded for the homogenization of the vapour phase to the liquid phase, i.e., “vapour bubble” disappearance (Fig. 30). Consequently, Type 1 brine-rich and Type 3 vapour-rich fluid

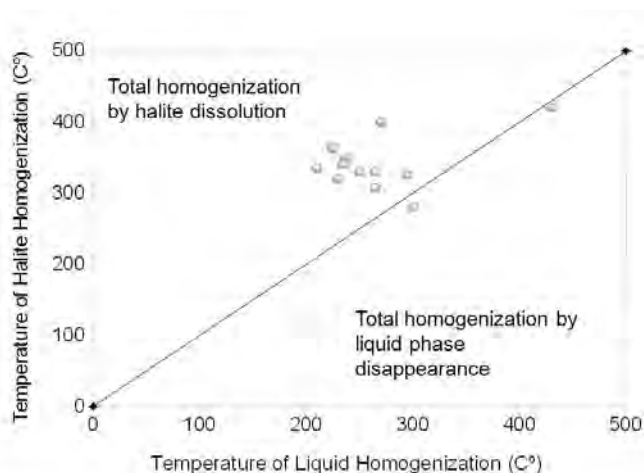


Fig. 30. Homogenization characteristics of Three Firs Type 1 fluid inclusion assemblages. Each symbol is a FIA that represents an average value of 3 to 11 individual inclusions. Symbols size is approximately equal to the error ($\pm 10\%$) of the measured homogenization temperature. Note that Three Firs Type 1 inclusions are almost exclusively homogenized by halite dissolution.

inclusions cannot represent the immiscible endmembers of a single phase (supercritical) fluid unmixing on the H₂O-NaCl solvus as explained in Bodnar and Vityk (1994). This finding is consistent with the lack of petrographic evidence for fluid unmixing. Specifically, Type 1 brine-rich and Type 3 vapour-rich inclusions never occur together in the same trail or cluster as would be expected during fluid unmixing (Roedder, 1984). Consequently, the total homogenization temperatures measured only represent minimum estimates of the trapping temperature. The fact that Type 1 and Type 3 inclusions were trapped in the same quartz grain but are not in chemical equilibrium, suggests that aqueous brines and vapours have migrated from their original sites of fluid unmixing. This non-equilibrium trapping of immiscible vapour and brines is recognized in other porphyry systems, for example the Early Jurassic Kerness South porphyry Cu-Au deposit in the Toodoggonne district (Duuring et al., 2009a) and the Bingham and Butte porphyry Cu-Mo \pm Au deposits in Utah and Montana, respectively (Rusk et al., 2008 and references therein). The “mixed” Type 2 liquid-rich fluid inclusions are interpreted to be mechanical (i.e., non-equilibrium) mixtures of Type 1 brines and Type 3 vapours circulating in the Three Firs hydrothermal system. Consequently, they cannot be used to infer physicochemical conditions of ore formation and were not measured.

Total homogenization temperatures for primary and pseudosecondary fluid inclusions in stage 3 quartz-hornblende-sulphide \pm K-feldspar veins range from 295 to 400° C with corresponding pressures ranging between 0.6 and 2.5 kbar (Fig. 31). These temperatures and pressures are minimum estimates because the true trapping pressure and temperature will lie somewhere higher along the projected isochores calculated for the individual FIAs. Assuming a lithostatic load of 3.3 km/kbar (Hagemann and Brown, 1996), a minimum calculated pressure of 1.1 kbar corresponds to a formational depth of 3.6 km for stage 3 veins in sample MAG12-03-172.9 (Fig. 31a). For stage 3 veins in sample MAG12-05-274.1 a minimum calculated pressure of 0.6 kbar corresponds to a minimum formational

Table 2. Summary of microthermometric data from the Three Firs veins. Microthermometric methods are described in the text. Salinities (equiv. wt.% NaCl) were calculated using the Bodnar and Vityk (1994) equations of state for the H₂O-NaCl-KCl system.

FIA	Sample Chip	Petrographic Description at STP	Type of Inclusion	Vol % (Vapor)	Th (°C) (L-V)	Th Halite (°C)	Tm Ice (°C)	Salinity %wt
Stage 4 vein: Qtz-hbl-ccp-py ± carb ± mag ± ep ± chl (medial sutures)								
		Quartz hosts randomly arranged, equant- to negative crystal-shaped, brine-rich, pseudosecondary inclusions that contain a halite daughter crystal and a second translucent mineral (carbonatesylwite?)	Brine rich	10-15%	295°C ± 3°C (L)	325°C ± 15°C	-38°C ± 2°C	40.1
D (n=7)	MAG12-05-302.5-C4							
E (n=6)	MAG12-05-302.5-C5	Quartz hosts randomly arranged, irregular- to negative crystal-shaped, brine-rich, pseudosecondary inclusions that contain a halite daughter crystal and sometimes two translucent minerals (carbonatesylwite?)	Brine rich	10-15%	237°C ± 5°C (L)	350°C ± 5°C	-39°C ± 2°C	42.4
F (n=4)	MAG12-05-302.5-C5	Quartz hosts randomly arranged, irregular- to negative crystal-shaped, brine-rich, pseudosecondary inclusions that contain a halite daughter crystal and a second translucent sub-rounded mineral (sylwite?)	Brine rich	10-15%	430 ± 5°C (L)	420 ± 5°C	-40°C ± 5°C	49.6
Stage 4 vein: Qtz-hbl-ccp-py ± carb ± mag ± ep ± chl (medial sutures)								
		Quartz hosts linearly arranged, equant to negative crystal shaped, brine rich, primary inclusions with a halite daughter crystal and small translucent solid (carbonate), oriented about a growth margin proximal to chalcocopyrite grain	Brine rich	10-25%	270°C ± 20°C (L)	400°C ± 20°C	-40 ± 5°C	47.4
K (n=8)	MAG12-03-164.75-C1							
L (n=6)	MAG12-03-164.75-C2	Quartz hosts linearly arranged, equant to negative crystal shaped, two-phase, liquid rich, several appear to have small cubic solid (halite?) pseudosecondary inclusions proximal to a chalcocopyrite grain.	Brine rich	15-20%	240°C ± 5°C (L)	250 ± 10°C	-28°C ± 2°C	34.6
O (n=4)	MAG12-03-164.75-C4	Quartz hosts randomly arranged, equant- to negative crystal-shaped, brine-rich, pseudosecondary inclusions that contain a halite daughter crystal and a second translucent mineral (carbonatesylwite?)	Brine rich	10-15%	300°C ± 5°C (L)	280°C ± 10°C	-40°C ± 6°C	36.6
R (n=7)	MAG12-03-164.75-C6	Quartz hosts randomly arranged, equant- to negative crystal-shaped, brine-rich, pseudosecondary inclusions that contain a halite daughter crystal and a second translucent mineral (carbonatesylwite?) proximal to sulphide grain	Brine rich	10-15%	250°C ± 10°C (L)	330°C ± 15°C	-40°C ± 5°C	40.6
Stage 3 vein: Qtz-hbl-ccp-py ± carb ± mag ± ep ± chl ± k sp								
		Quartz hosts randomly arranged, irregular to negative crystal shaped, brine rich, pseudosecondary inclusions with a halite daughter crystal and one or two small translucent solids (carbonate and or sylwite), proximal to chalcocopyrite grain	Brine rich	10-15%	265°C ± 5°C (L)	330°C ± 15°C	-38°C ± 7°C	40.1
U (n=11)	MAG12-05-172.90-C1							
W (n=11)	MAG12-05-172.90-C2	Quartz hosts randomly arranged, equant- to negative crystal-shaped, brine-rich, primary inclusions that contain a halite daughter crystal and a second translucent mineral (carbonate/sylwite?) proximal to chalcocopyrite grain	Brine rich	10-15%	210°C ± 10°C (L)	335°C ± 15°C	-43°C ± 5°C	41.0
Z (n=6)	MAG12-05-172.90-C5	Quartz hosts randomly arranged, irregular to negative crystal shaped, brine rich, pseudosecondary inclusions with a halite daughter crystal and one or two small translucent solids (carbonate and or sylwite)	Brine rich	10-15%	225°C ± 5°C (L)	365°C ± 8°C	-30°C ± 5°C	43.8
AB (n=5)	MAG12-05-172.90-C6	Quartz hosts randomly arranged, irregular to negative crystal shaped, brine rich, pseudosecondary inclusions with a halite daughter crystal and one or two small translucent solids (carbonate and or sylwite) quartz embayed by pyrite grain.	Brine rich	5-10%	265°C ± 5°C (L)	307°C ± 10°C	-37°C ± 5°C	38.7
Stage 3 vein: Qtz-hbl-ccp-py ± carb ± mag ± ep ± chl ± k sp								
		Quartz hosts randomly arranged, irregular to negative crystal shaped, brine rich, pseudosecondary inclusions with a halite daughter crystal and one or two small translucent solids (carbonate and or sylwite)	Brine rich	10-12%	225°C ± 5°C (L)	362°C ± 8°C	-42°C ± 5°C	43.5
AE (n=6)	MAG12-03-274.12-C1							
AF (n=5)	MAG12-03-274.12-C2	Quartz hosts randomly arranged, equant, brine rich, pseudosecondary inclusions with a halite daughter crystal and small translucent solid (carbonate)	Brine rich	5-20%	235°C ± 5°C (L)	340°C ± 10°C	-34°C ± 5°C	41.4
AL (n=3)	MAG12-03-274.12-C4	Quartz hosts randomly arranged, equant to negative crystal shaped, brine rich, pseudosecondary inclusions with a halite daughter crystal, one or two small translucent solids (carbonate and or sylwite) and daughter sulphide (triangular opaque)	Brine rich (S)	10-12%	265°C ± 5°C (L)	404°C ± 3°C	-41°C ± 4°C	47.8
AM (n=4)	MAG12-03-274.12-C4	Quartz hosts randomly arranged, equant to negative crystal shaped, brine rich, pseudosecondary inclusions with a halite daughter crystal and one or two small translucent solids (carbonate and or sylwite)	Brine rich	5-20%	302°C ± 18°C (L)	295°C ± 15°C	-40°C ± 5°C	37.7
AQ (n=4)	MAG12-03-274.12-C7	Quartz hosts randomly arranged, equant to negative crystal shaped, brine rich, pseudosecondary inclusions with a halite daughter crystal	Brine rich	5-10%	230°C ± 5°C (L)	320°C ± 5°C	n/a	39.7

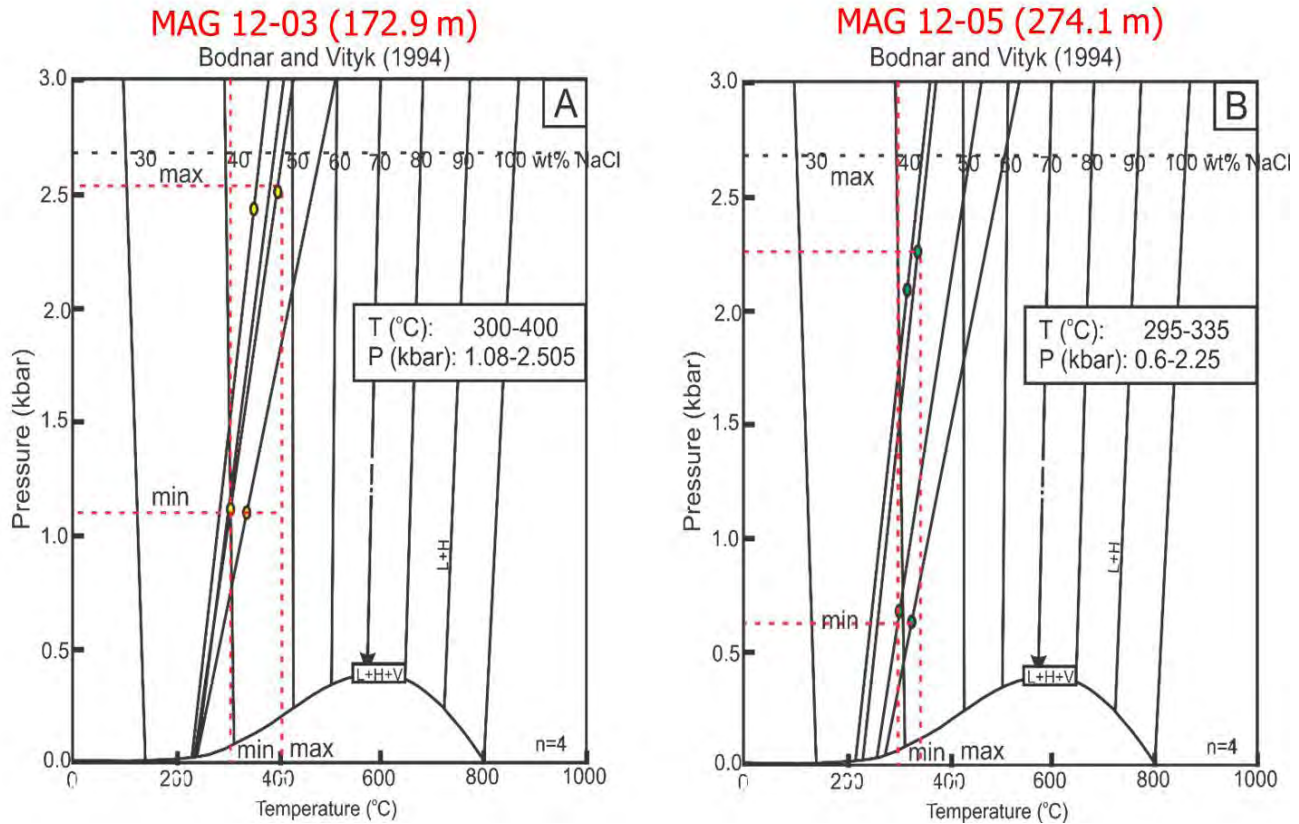


Fig. 31. Pressure-temperature diagrams showing calculated isochores for each FIA using the Bodnar and Vityk (1994) equations of state. These isochores allow estimating P-T trapping condition in stage 3 veins. **a)** Sample MAG12-03 172.9 m. **b)** Sample MAG12-05 274.1 m.

depth of 2.0 km (Fig. 31b). The higher pressures calculated for several FIA's in stage 3 veins (2.5 kbar in MAG12-03-172.9 and 2.3 kbar in MAG12-05-274.1) correspond to formational depths of 7 or 8 km, which is deeper than most porphyry deposits, although Butte porphyry Cu deposit in Montana was purportedly formed at 9 km (Rusk et al., 2008).

Stage 4 quartz-hornblende-sulphide veins host primary and pseudosecondary fluid inclusions with total homogenization temperatures that range from 250 to 420° C (Table 2) with corresponding pressures ranging between 0.6 to 2.6 kbar (Fig. 32). Similar to the stage 3 veins, these temperatures and pressures are minimum estimates. True trapping pressures and temperatures will fall somewhere higher along the projected isochores calculated for the individual FIAs. Assuming a lithostatic load of 3.3 km/1 kbar, a minimum calculated pressure of 0.6 kbar corresponds to a formational depth of 2.0 km for stage 4 veins in sample MAG12-03-164.7 (Fig. 32a). For stage 4 veins in sample MAG12-05-302.5 (Fig. 32b), a minimum calculated pressure of 1.4 kbar corresponds to a formational depth of 4.6 km. The higher pressures calculated for several FIA's in stage 4 veins (2.0 kbar in MAG12-03-164.7 and 2.6 kbar in MAG12-05-302.5) correspond to formational depths in excess of 8 km, several kilometres deeper than most porphyry deposits (e.g., Sillitoe, 2010).

In summary, the microthermometric data suggest that the main stages of Cu-Au mineralization (the stage 3 and 4 veins) occurred at depths between 2 and 4.6 km and at temperatures from ~ 300 to 400° C using minimum pressure-temperature

estimates. This is the expected pressure-temperature range for the formation of porphyry Cu-Mo-Au deposits and accords well with the style of veins, types of alteration, and geological features at the Three Firs prospect. Although calculated pressures are imprecise, the steep positive slope of the isochores means that the temperatures measured are close ($\pm 30^\circ$ C) to the true trapping temperatures (Bodnar and Vityk, 1994).

The high salinities and pressures calculated for some FIAs in Main stage veins at Three Firs likely do not record the actual P-T-X conditions of mineralization for several reasons. First, the equations of state used to calculate isochores are inherently inaccurate at high salinities (> 50 wt.% NaCl) and pressures (> 2.0 kbar), resulting in potentially erroneous thermodynamic estimates of pressure and temperature (Becker et al., 2008). Second, FIAs that exhibit very high salinities (> 50 equiv. wt.% NaCl) may be the result of post-entrapment water loss along microfractures resulting in a change in volume and increased salinity, hence they do not represent original fluid compositions. Third, we may have incorporated inclusions into a FIA that are not part of a single discrete fluid event. Finally, we may have measured fluid inclusions that were opened (decrepitated) and subsequently re-sealed with little visible evidence that they were modified after entrapment.

8. Alteration reflectance spectroscopy

Spectral Evolution's ^(TM) SpecTERRA reflectance spectroscopy was used to identify clay alteration minerals and gain a better understanding of hydrothermal alteration at

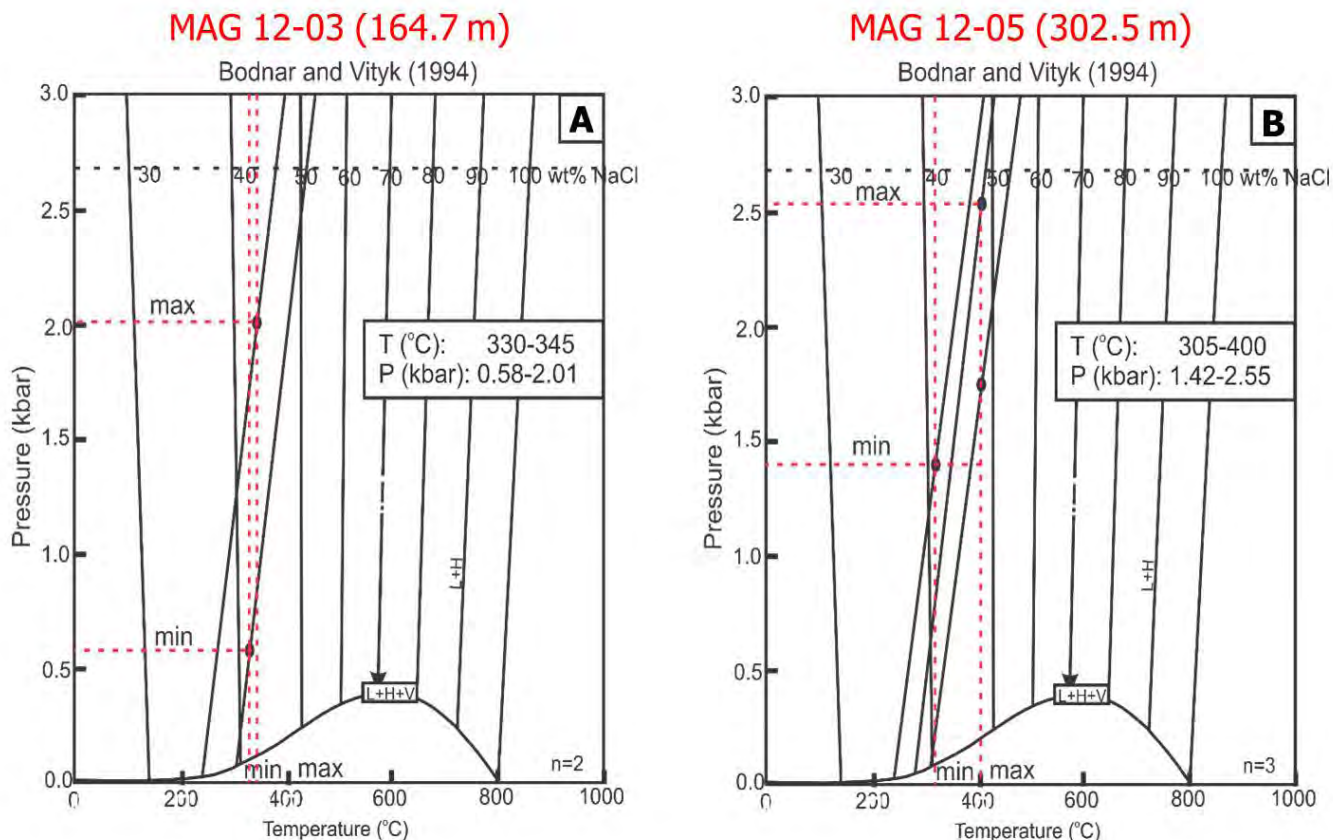


Fig. 32. Pressure-temperature diagrams showing calculated isochores for each FIA using the Bodnar and Vityk (1994) equations of state. These isochores permit estimating P-T trapping condition in stage 4 veins. **a)** Sample MAG12-03-164.7 m. **b)** Sample MAG12-05-302.5 m.

the Three Firs prospect. Clay minerals are typically too fine grained to identify in thin section, and reflectance spectra data are necessary to fully characterize mineralogy. Every mineral has its own characteristic reflectance spectra, which reflects physiochemical bonds in a mineral's crystal structure. By analyzing the position and shape of spectral features, minerals can be identified and, based on the sharpness or depth of a given spectral feature, their crystallinity established.

The reflectance data were collected on three targets in a sample interval. A comprehensive 43-element assay data for the same interval allowed for robust interpretation and comparison. Care was taken to avoid analyzing targets that were dusty or wet, which would have resulted in erroneous spectra. Where possible, targets were selected after geological interpretation and identification of minerals in hand sample. Spectra for each target were subsequently uploaded for interpretation using DarWin and SpecMin software packages.

Our reflectance spectroscopy work revealed piemontite, clinocllore, hydromuscovite, illite-smectite interlayers, and crystalline illite (Figs. 33 a-e); crystalline kaolinite was identified by Spectral Evolution geologists (Kari Wurst, pers. comm. 2013). Crystalline illite is a white mica commonly associated with sericite and muscovite in phyllic alteration zones generated by relatively hot ($> 220^{\circ}\text{C}$), moderately acidic hydrothermal fluids (e.g., Reyes, 1990; Ji and Brown, 2000). Crystalline kaolinite is typically associated with argillic alteration zones that form at slightly lower temperatures ($> 200^{\circ}\text{C}$) and moderate acidities (e.g., White and Hedenquist,

1995; Seedorff et al., 2005). Both illite and kaolinite can form under near-surface conditions at very low temperatures, but with a low crystallinity. Thus, the identification of crystalline illite and kaolinite confirms that they represent hydrothermal alteration phases and are not the products of present-day surface weathering. Clinocllore is a Mg-rich chlorite associated with propylitic alteration and stage 7 (late) mineralized veins at Three Firs. It also may pre-date Cu-Au mineralization and have formed via contact and/or regional metamorphism. Consequently, a complete understanding of the origins of clinocllore at Three Firs awaits further study.

Piemontite, a Ca-rich clinzoisite (epidote group) mineral, implies Ca-rich hydrothermal alteration at temperatures $> 240^{\circ}\text{C}$ (e.g., White and Hedenquist, 1995). Consequently, hydrothermal piemontite could belong to both the calc-potassic and propylitic alteration assemblages at Three Firs.

9. Discussion and conclusions

9.1. Prospect geology

Because the Three Firs Cu-Au prospect is a new discovery our geological understanding is still at a rudimentary stage. Nonetheless, our study indicates that the prospect displays most of the key elements found in classic northern Cordilleran calc-alkaline porphyry Cu-Au (Mo) deposits. The most intense alteration and highest metal grades are spatially and temporally associated with a series of monzonite dikes that are part of a more extensive suite of granitic dikes. The different types of veins ("M", "A", "B", and "D" varieties) and associated

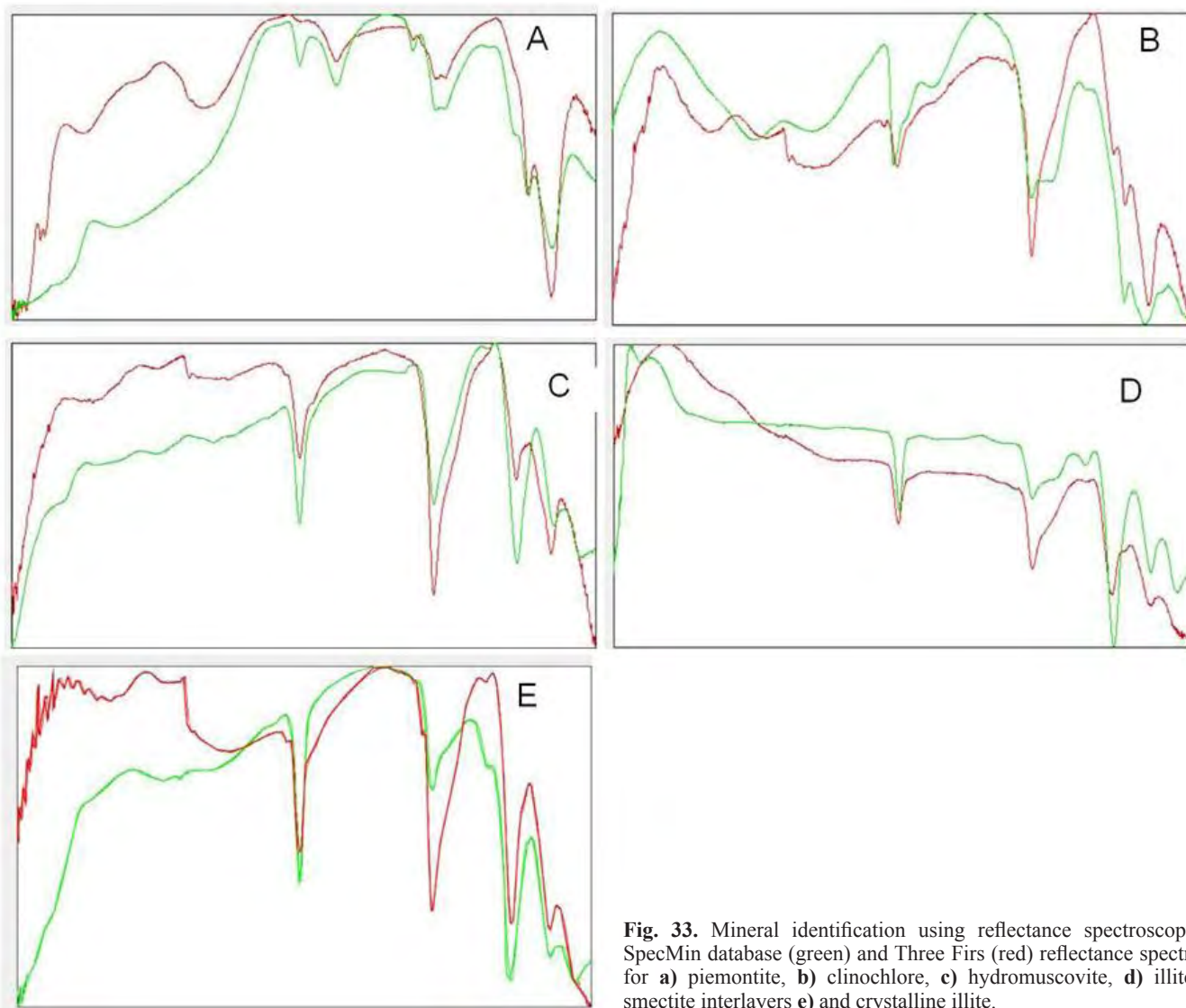


Fig. 33. Mineral identification using reflectance spectroscopy. SpecMin database (green) and Three Firs (red) reflectance spectra for **a)** piemontite, **b)** clinocllore, **c)** hydromuscovite, **d)** illite-smectite interlayers **e)** and crystalline illite.

styles of alteration (potassic, phyllic, calc-potassic, propylitic, and carbonate) are also characteristic of medium- to high-K, calc-alkaline porphyry Cu-Au-(Mo) deposits in the northern Cordillera (e.g., Seedorff et al., 2005). Eight stages of vein formation were identified, beginning with pre-mineralization, through early, main and late mineralization, ending with post-mineralization. These stages represent separate but partially overlapping fluid events with the main stages (3, 4, and 5) producing most of the Cu-Au mineralization. A suite of rocks samples collected from drill core for whole-rock geochemistry and reflectance spectrometry confirm that Three Firs is related to medium-K, calc-alkaline magmas that formed in a volcanic arc environment.

9.2. Evolution of the magmatic-hydrothermal mineral system at Three Firs

Fluid inclusion studies indicate that the main stages of Cu-Au sulphide mineralization occurred at depths between 2 and 4.6 km, and at temperatures between 300 and 400° C. This temperature range corresponds to where Cu solubility (as

CuCl₂) drops by ~ 95% in a normal porphyry ore fluid (e.g., Hezarkhani et al., 1999). Calculations by Hezarkhani et al. (1999) indicate that Cu solubility at 400° C is approximately 1000 ppm whereas at 350° C it is only 25 ppm. Thus, the focussed deposition of Cu (Au) sulphides in “A” veins (stage 3) and “B” veins (stage 4) is to be expected, based on the dramatic decrease in Cu solubility during the formation of these main stage veins. These Cu solubility studies also provide a reason why subsequent stages of vein formation contain much less Cu: they formed from “spent” fluids that deposited virtually all their Cu at higher temperatures. Rare native Au in grains of disseminated chalcopyrite-bornite in altered wall-rock surrounding later (cooler?) stage 5 “D” veins may be attributable to the greater solubility of Au compared to Cu at lower temperatures. Gammons and Williams-Jones (1997) have shown that Au is dissolved mainly as AuCl₂⁻ at high temperatures, and solubilities decrease steadily with cooling. At lower temperatures, the predominant complex eventually switches to Au(HS)₂⁻, at which point Au solubility may actually increase with cooling. The specific temperature of the chloride-

bisulphide transition in porphyry systems depends on the pH, the H_2S/Cl ratio of the original fluid, and whether or not boiling (fluid unmixing) has occurred (Gammons and Williams-Jones, 1997).

Isochores calculated from the equations of state in Bodnar and Vityk (1994) indicate that fluid inclusions were trapped at pressures ranging from 0.6 kbar to 1.42 kbar, which correspond to 2 to 4.6 km depth, assuming a lithostatic load. The assumption of lithostatic rather than hydrostatic load is justified, given the lack of fluid inclusion evidence for boiling, which only occurs under hydrostatic conditions (e.g., Haas, Jr., 1976). As discussed above, the lack of boiling during vein formation at Three Firs is indicated by the homogenization behaviour of halite in Type 1 aqueous fluid inclusions. In addition to the pressure estimates from fluid inclusions, evidence that Three Firs is a relatively deep-seated porphyry system comes from the lack of phreatic and magmatic-hydrothermal breccias (e.g., Sillitoe, 1985), absence of bladed quartz after calcite in the veins (Simmons and Christiansen, 1984), and simple crustification textures in the main stage veins that imply only one or two episodes of open-space filling. Finally, shallow (< 2 km) Au-rich epithermal zones have not been intersected in any holes drilled into the Three Firs prospect, although we have identified rare native Au (Fig. 19) and elevated Au abundances (up to 23 g/t Au) are found in small intervals (Sherlock et al., 2013).

9.3. Comparison to other porphyry prospects in the Woodjam district and elsewhere in the Canadian Cordillera

It has been suggested that the Woodjam district hosts both calc-alkaline and alkalic styles of porphyry Cu-Au mineralization (e.g., Blackwell et al., 2012a; del Real et al., 2013; Sherlock et al., 2013). This study demonstrates that Three Firs is a calc-alkaline porphyry Cu-Au deposit with many similarities to the Southeast Zone and Takom prospects. It also shares similarities with the Deerhorn (Scott, 2012; del Real et al., 2013) and Megabuck prospects, both of which have been tentatively identified as alkalic porphyry systems. Although work on these two porphyry systems is at an early stage, published studies on the types of alteration and styles of veins reveal many more similarities than differences amongst all the prospects (del Real et al., 2013). Moreover, the monzonite dikes associated with the Deerhorn porphyry prospect have been shown to be calc-alkaline and not alkalic intrusions (Scott, 2012). The ages of felsic intrusions associated with porphyry prospects in the Woodjam camp (Fig. 3) are also consistently younger than the alkalic intrusions that comprise the Late Triassic Copper Mountain suite (206-200 Ma). With few exceptions (Takom?), the U-Pb (zircon) ages of intrusions and Re-Os (molybdenite) ages of mineralization are < 200 Ma, consistent with magmatism in the Woodjam district being exclusively related to different phases of the Late Triassic-Early Jurassic (~203-193 Ma) Takomkane batholith (Scharizza et al., 2009; Logan et al., 2011; Blackwell et al., 2012a).

Other calc-alkaline porphyry deposits in British Columbia with similarities to the Three Firs prospect include the Late Jurassic porphyry Cu-Au±Mo deposits (Kemess South, Kemess North and Pine) in the Toadoggonne district (Duuring et al., 2009a, b), the Late Triassic Schaft Creek Cu-Mo-(Au) deposit in the Stikine arch (Scott et al., 2008), and the Late

Cretaceous porphyry Cu±Mo±Au deposits (Huckleberry and Seel) associated with the Bulkley Intrusive Suite in the Skeena arch (Jackson and Illerbrun, 1995; McDowell and Giroux, 2012).

9.4. Implications for further exploration

This study demonstrates that the Three Firs prospect formed in a pressure-temperature “window” that is optimal for the deposition of Cu and Au. Consequently, future exploration should continue to focus on the current Three Firs area and its immediate environs. It is unlikely that the bulk of the deposit remains undiscovered at depth because Cu and Au would have been in solution as soluble chloride complexes at the higher temperatures found in a porphyry root zone at depths of 4-5 km. The Au solubility studies allow that a slightly Au enriched zone could lie immediately above the current level of Cu-Au mineralization, but as discussed, there is no evidence for the development of high-grade, epithermal vein-style Au (Ag) zones. The Three Firs system is probably too deep.

On a regional scale, it may be worthwhile to reconsider the proposal that the Woodjam district hosts both alkalic and calc-alkaline styles of porphyry Cu-Au deposits. The geological, geochemical, and geochronological evidence is equivocal. A simpler model that considers all porphyry prospects to be high- to medium-K, calc-alkaline systems that formed from different intrusive phases of the Takomkane batholith removes the vexing problem of explaining how both alkalic and calc-alkaline porphyry systems form at the same time in the same place (e.g., Lang et al., 1995). To our knowledge there is no other porphyry camp in the world where this situation exists. A model invoking only calc-alkaline porphyry Cu-Au±Mo deposits in the Woodjam district is also more consistent with the easterly migrating Mesozoic magmatic arc proposed for the southern Nicola (Logan et al., 2011). According to this model, any alkalic porphyry Cu-Au deposits of the Late Triassic-Early Jurassic Copper Mountain suite should lie to the west of the younger calc-alkaline porphyry Cu-Au±Mo deposits of the Early Jurassic Takomkane suite at Woodjam. There is no requirement to have these two magmatic belts somehow converge and overlap in the Woodjam district.

Acknowledgments

This study is the result of a B.Sc. Honours thesis done by S. Vandekerkhove at the University of Victoria in 2012-2013, under the supervision of Drs. S. M. Rowins and S.T. Johnston. Gold Fields Canada, the British Columbia Geological Survey and the University of Victoria are all thanked for funding various aspects of this project and providing access to laboratory facilities. Gold Fields geologists Ross Sherlock, Twila Skinner, Amelia Rainbow, Jacqueline Blackwell, Matt Eckfeldt, Irene del Real, and Julia Scott are thanked for insightful discussions on the geology of the Three Firs prospect and the Woodjam district. Larry Aspler is thanked for a thorough review of the paper, which helped to clarify content and presentation. Finally, thanks go to friends and family of S. Vandekerkhove for their unstinting support during completion of this study.

References cited

Bailey, D.G., Bloodgood, M.A., Campbell, R.B., Panteleyev, A., Hancock, K.D., and Struik, L.C., 1990. Geology of the central

- Quesnel Belt British Columbia NTS 93A/5, 6, 7, 11, 12, 13; 93B/9, 16; 93G/1; 93H/4; British Columbia Geological Survey Bulletin 97, Map 1, scale 1:100 000, 1 sheet.
- Beane, R.E., and Tittley, S.R., 1981. Porphyry copper deposits. Part II. Hydrothermal alteration and mineralization. *Economic Geology* 75th Anniversary Volume, p.235-269.
- Becker, S.P., Fall, A., Bodnar, R.J., 2008. Synthetic fluid inclusions. XVII. PVTX properties of high salinity H₂O-NaCl solutions (> 30 wt.% NaCl): Application to fluid inclusions that homogenize by halite disappearance from porphyry copper and other hydrothermal ore deposits. *Economic Geology*, 103, 539-554.
- Blackwell, J., Black, E. and Skinner, T., 2012a. National Instrument 43-101 Technical Report on 2011 activities on the Woodjam North Property, Cariboo Mining Division, British Columbia, Internal report prepared for Woodjam Consolidated Copper Corp., 134 p.
- Blackwell, J.L., Lesage, G., Skinner, T., Eckfeldt, M., Black, E., Hamilton, J., Hertel, J., Laird, B., Madson, J., Rainbow, A., Sherlock, R., and Sepp, M., 2012b. Geology of the Woodjam Property core area, Gold Fields Internal Document, 15 p.
- Bodnar, R.J., 1994. Synthetic fluid inclusions. XII: The system H₂O-NaCl. Experimental determination of the halite liquidus and isochores for a 40 wt.% NaCl solution. *Geochimica et Cosmochimica Acta*, 58, 1053-1063.
- Bodnar R.J., and Vityk, M.O., 1994. Interpretation of microthermometric data for NaCl-H₂O fluid inclusions. In: De Vivo B., and Frezzotti M.L. (Eds.), *Fluid inclusions in minerals: methods and applications*. Virginia Polytechnic Institute and State University, Blacksburg, pp. 117-131.
- Corbett, G.J., and Leach, T.M., 1998. Southwest Pacific Rim gold-copper systems: Structure, alteration, and mineralization. *Society of Economic Geologists Special Publication* 6, 154-182.
- del Real, I., Hart C.J.R., Bouzari, F., Blackwell, J.L., Rainbow, A., Sherlock, R., and Skinner, T., 2013. Paragenesis and alteration of the Southeast Zone and Deerhorn deposits, Woodjam Property, Central British Columbia (Part of 093A). In: *Geoscience BC Summary of Activities 2012*. Geoscience BC Report 2013-01, 79-90.
- Duuring, P., Rowins, S.M., McKinley, B.S.M., Dickinson, J.M., Diakow, L.J., Young-Seog, K., and Creaser, R.A., 2009a. Magmatic and structural controls on porphyry-style Cu-Au-Mo mineralization at Kemess South, Toodoggone District of British Columbia, Canada. *Mineralium Deposita*, 44, 435-462.
- Duuring, P., Rowins, S.M., McKinley, B.S.M., Dickinson, J.M., Diakow, L.J., Young-Seog, K., and Creaser, R.A., 2009b. Examining potential genetic links between Jurassic porphyry Cu-Au±Mo and epithermal Au±Ag mineralization in the Toodoggone District of north-central British Columbia, Canada. *Mineralium Deposita*, 44, 463-496.
- Gabrielse, H., and Yorath, C.J., 1991. Introduction. Chapter 1. In: Gabrielse, H., and Yorath, C.J., (Eds.), *Geology of the Canadian Cordilleran Orogen in Canada*, Geological Survey of Canada, *Geology of Canada*, no. 4., pp. 3-11.
- Gammons, C.H., and Williams-Jones, A.E., 1997. Chemical mobility of gold in the porphyry-epithermal environment. *Economic Geology*, 92, 45-59.
- Goldstein R.H., and Reynolds, T.J., 1994. Systematics of Fluid Inclusions in Diagenetic Minerals. *Society for Sedimentary Geology Short Course* 31, 199 p.
- Hagemann S.G., and Brown P.E., 1996. Geobarometry in Archean lode gold deposits. *European Journal of Mineralogy*, 8, 937-960.
- Haas, J.L., 1976. Physical properties of the coexisting phases and the thermochemical properties of the H₂O component in boiling NaCl solutions. *U.S. Geological Survey Bulletin*, 1421-A, 73 p.
- Hezarkhani, A., Williams-Jones, A. E., & Gammons, C. H., 1999. Factors controlling copper solubility and chalcopyrite deposition in the Sungun porphyry copper deposit, Iran. *Mineralium Deposita*, 34, 770-783.
- Ji J., and Browne, P. R., 2000. Relationship between illite crystallinity and temperature in active geothermal systems of New Zealand. *Clays and Clay Minerals*, 48, 139-144.
- Lang, J.R., Stanley, C.R., and Thompson, J.F.H., 1995. Porphyry copper-gold deposits related to alkalic igneous rocks in the Triassic-Jurassic arc terranes of British Columbia. In: Wahl Pierce, F., and Bolm, J.G., (Eds.), *Porphyry Copper Deposits of the American Cordillera*, Arizona Geological Society, *Digest* 20, pp. 219-236.
- Lemaitre, R.W., 1978. The chemical variability of some common igneous rocks. *Journal of Petrology*, 17, 589-637.
- Logan, J.M., 2013. Porphyry systems of central and southern BC: Overview and field trip road log. In: Logan, J.M. and Schroeter, T.G., (Eds.), *Porphyry Systems of Central and Southern BC: Prince George to Princeton*. Society of Economic Geologists *Guidebook* 44, pp. 1-45.
- Logan, J.M., Mihalynuk, M., Ullrich, T., and Friedman, R.M., 2007. U-Pb ages of intrusive rocks and ⁴⁰Ar/³⁹Ar plateau ages of copper-gold-silver mineralization associated with alkaline intrusive centres at Mount Polley and the Iron Mask batholith, southern and central British Columbia: In: *Geological Fieldwork 2006*, British Columbia Ministry of Energy, Mines and Petroleum Resources, British Columbia Geological Survey Paper 2007-1, pp. 93-116.
- Logan, J.M., Mihalynuk, M.G., Friedman, R.M., and Creaser, R.A., 2011. Age constraints of mineralization at the Brenda and Woodjam Cu-Mo +/- Au porphyry deposits - an Early Jurassic calc-alkaline event, south-central British Columbia. B.C. In: *Geological Fieldwork 2010*, British Columbia Ministry of Forests, Mines and Land, British Columbia Geological Survey Paper 2011-1, pp. 129-143.
- Lowell, J. D., & Guilbert, J. M., 1970. Lateral and vertical alteration-mineralization zoning in porphyry ore deposits. *Economic Geology*, 65, 373-408.
- McDowell, C., and Giroux, G., 2012. Mineral resource estimate update for the Seel copper-gold porphyry deposit, 43-101 report, 136 p.
- McMillan, W.J., 2005. Porphyry Cu-Mo deposits of the Highland Valley district, Guichon Creek batholith, British Columbia, Canada. In: Porter, T.M. (Ed.), *Super Porphyry Copper & Gold Deposits: A Global Perspective*, PGC Publishing, Adelaide, 1, pp. 259-274.
- McMillan, W.J., Thompson, J.F.H., Hart, C.J.R., and Johnston, S.T., 1995. Regional geological and tectonic setting of porphyry deposits in British Columbia and Yukon Territory. In: Schroeter, T.L. (Ed.), *Porphyry Deposits of the Northwestern Cordillera of North America*, Canadian Institute of Mining and Metallurgy *Special Volume* 46, pp. 40-57.
- Monger, J.W.H., Souther, J.G., and Gabrielse, H., 1972. Evolution of the Canadian Cordillera: A plate-tectonic model. *American Journal of Science*, 272, 577-602.
- Nelson, J.L., Colpron, M., and Israel, S., 2013. The Cordillera of British Columbia, Yukon, and Alaska: Tectonics and metallogeny. In: Colpron, M., Bissig, T., Rusk, B.G., and Thompson, J.F.H. (Eds.), *Tectonics, Metallogeny, and Discovery: The North American Cordillera and Similar Accretionary Settings*. Society of Economic Geologists *Special Publication* Number 17, pp. 53-110.
- Panteleyev, A., Bailey, D.G., Bloodgood, M.A., and Hancock, K.D., 1996. Geology and mineral deposits of the Quesnel River-Horsefly map area, central Quesnel Trough, British Columbia NTS map sheets 93A/5, 6, 7, 11, 12, 13; 93B/9, 16; 93G/1; 83H/4; British Columbia Geological Survey Bulletin 97, 156 p.
- Pearce, J. A., Harris, N. B., and Tindle, A. G., 1984. Trace element discrimination diagrams for the tectonic interpretation of granitic rocks. *Journal of Petrology*, 25, 956-983.
- Peccerillo, A., and Taylor, S. R., 1976. Geochemistry of Eocene calc-alkaline volcanic rocks from the Kastamonu area, northern Turkey. *Contributions to Mineralogy and Petrology*, 58, 63-81.
- Preto, V.A., 1977. The Nicolo Group: Mesozoic volcanism related to rifting in southern British Columbia. In: Baragar, W.R., Coleman, L.C., and Hall, J.M., (Eds.), *Volcanic Regimes in Canada*.

- Geological Association of Canada Special Paper 16, pp. 39-57.
- PriceWaterhouseCooper, 2012. Stay the course: The mining industry in British Columbia 2012. 28 p.
- Reyes, A.G., 1990. Petrology of Philippine geothermal systems and the application of alteration mineralogy to their assessment. *Journal of Volcanology and Geothermal Research*, 43, 279-309.
- Roedder, E. 1984. Fluid Inclusions. *Reviews in Mineralogy Volume 12*, 644 p.
- Rusk, B.G., Reed, M.H., and Dilles, J.H., 2008. Fluid inclusion evidence for magmatic-hydrothermal fluid evolution in the porphyry copper-molybdenum deposit at Butte, Montana. *Economic Geology*, 103, 307-334.
- Schiarizza, P., Bell, K., Bayliss, S., 2009. Geology and mineral occurrences of the Murphy Lake area, south-central British Columbia (NTS 093A/03). In: British Columbia Ministry of Mines, Energy and Petroleum Resources, *Geological Fieldwork 2008*, British Columbia Geological Survey Paper 2009-1, pp. 169-188.
- Scott, J.E., Richards, J.P., Heaman, L.M., Creaser, R.A., and Salazar, G.S., 2008. The Schaft Creek porphyry Cu-Mo-(Au) deposit, northwestern British Columbia. *Exploration and Mining Geology*, 17, 163-196.
- Seedorff, E., Dilles, J.H., Proffett Jr., J.M., Einaudi, M.T., Zurcher, L., Stavast, W.J.A., Johnson, D.A., and Barton, M.D., 2005. Porphyry deposits: Characteristics and origin of hypogene features. In: Hedenquist, J.W., Thompson, J.F.H., Goldfarb, R.J., and Richards, J.P. (Eds.). *Economic Geology 100th Anniversary Volume*. Society of Economic Geologists, pp. 251-298.
- Shepherd, T.J., Rankin, A.H., Alderton, D.H.M., 1985. *A Practical Guide to Fluid Inclusion Studies*. Blackie, Glasgow, 239 p.
- Sherlock, R., Blackwell, J. and Skinner, T., 2013. National Instrument 43-101 Technical Report for 2012 Activities on the Woodjam North Property, Cariboo Mining Division, British Columbia, 275 p.
- Sillitoe, 1985. Ore-related breccias in volcanoplutonic arcs. *Economic Geology*, 80, 1467-1514.
- Sillitoe, R. H., 2010. Porphyry copper systems. *Economic Geology*, 105, 3-41.
- Simmons, S.F., and Christenson, B.W., 1984. Origins of calcite in a boiling geothermal system. *American Journal of Science*, 294, 361-400.
- Ulrich, T., Günther, D., & Heinrich, C. A., 2002. The evolution of a porphyry Cu-Au deposit, based on LA-ICP-MS analysis of fluid inclusions: Bajo de la Alumbrera, Argentina. *Economic Geology*, 97, p.1889-1920.
- Vandekerkhove, S., 2013. Mineral paragenesis, fluid inclusions and geochemistry of the Three Firs porphyry Cu-Au prospect: Woodjam porphyry Cu-Au district, British Columbia, Canada. B.Sc. (Honours) thesis, University of Victoria, 64 pages plus CD.
- White, N.C. and Hedenquist, J.W., 1995. Epithermal gold deposits: Styles, characteristics and exploration. *Society of Economic Geologists Newsletter Number 23*, p. 9-13.